Master of Science in Marine Biology

Climate change and the effect of darker coastal water on NCW euphotic zone properties - A theoretical study

Master thesis in theoretical ecology

Vilde Steinsdotter Ihler

Department of Biology
University of Bergen

November 2016

ACKNOWLEDGEMENTS

First of all I would like to thank my supervisor, Prof. Dag L. Aksnes for great support and guidance. He has been available 'round the clock', and provided me with constructive feedback. I would also like to thank Svein Rune Erga for providing me with data from some fjords along the Norwegian coast. Special thanks go to my friends, Magni and Helge, for good advices and for proofreading my thesis. Finally, I wish to express my gratitude to my fellow students, friends and family for support and encouragement throughout this whole process.

ABSTRACT

The Norwegian Coastal Water (NCW) derives from an extensive outflow of freshwater from the Baltic Sea and river runoff from the Norwegian coast, making the water less saline than the North Atlantic Water (NAW). Freshwater components contain relatively large amounts of dissolved organic substances that absorb light, which have been suggested to make the NCW darker than the NAW. Such substances may have both marine and terrestrial origin and are often referred to as chromophoric dissolved organic matter (CDOM). An increased CDOM concentration is predicted in the freshwater component of the NCW in the future, with possible implications on the biological ecosystem. The water column model of nutrient and phytoplankton of Huisman et al. (2006) was applied to analyse how NCW euphotic zone properties would respond to changes in CDOM attenuation in a past, present and future scenario. This model was originally parameterized for subtropical conditions, i.e. for oligotrophic waters. I investigated the extent to which the model could reproduce the vertical distribution of nutrients and phytoplankton under NCW conditions, i.e. more eutrophic waters, using data from previously published studies from three fjord locations along southern Norway. Further, published studies on Secchi depth observation and predicted future changes in terrestrial organic matter were used as a proxy for CDOM supply to the freshwater draining to the NCW. IMRs fixed hydrographic stations have been used as a proxy for changes in salinity and stratification. My results suggest that the NCW euphotic zone properties are susceptible to variation in CDOM attenuation. The estimated changes in the NCW euphotic zone properties are also suggested to be greater in the future than those estimated for the past. From two coastal stations, Lista and Sognesjøen, it was suggested a 5 meter reduction in the euphotic depth from the present to a future scenario. Elevated CDOM attenuation in the future is also expected to show eutrophication like symptoms. However, the simulations also indicated lower primary production which means more oligotrophy rather than eutrophy. Shoaling and narrowing of the euphotic habitat due to elevated CDOM concentration, and also due to higher concentration of phytoplankton in the surface water, may provide implications on the biological community.

TABLE OF CONTENTS

1 INTRODUCTION

1.1 Background

Previous studies have indicated that the Norwegian Coastal Water (NCW) has become darker during the last century (Aksnes et al., 2009; Dupont and Aksnes, 2013). Environmental changes expected throughout the future decades (Larsen et al., 2011a) predict more precipitation and warmer climate, bringing about vegetation changes on land (Larsen et al., 2011b). These progressions are expected to lead to an increased input of organic matter in rivers, thus also in the coastal water (Larsen et al., 2011a). A climate change scenario like this, with an increased supply of light-absorbing substances from catchments to surface waters, might have a great implications for the ecology of the water (Finstad et al., 2016; Larsen et al., 2011a) and may lead to an additional darkening of the coastal water, having an effect on its associated biological communities.

The NCW is a very important component in the fjords and coastal areas. Hence its properties and their impact on our coastal ecosystems are of great importance. The NCW differ from the North Atlantic Water (NAW) in that it has a lower salinity due to it containing a freshwater component that provides coastal water its characteristic properties. Freshwater components contain relatively large amounts of dissolved organic substances that absorb light, making the coastal waters darker than clear Atlantic waters.

Through theoretical analysis I will explore how euphotic zone properties of the Norwegian Coastal Water are expected to respond to increased light absorption i.e. darker coastal water, due to an increased supply of terrestrial organic material. Additionally, analyses of changes that might already have occurred are also considered.

1.2 The Norwegian Coastal Water

The NCW is transported with the Norwegian Coastal Current (NCC) all the way from Kattegat to the Barents Sea (Sætre, 2007) (Fig. 1). Sætre (2007) cited Helland-Hansen and Nansen from 1909: "*The coast water is on the whole moving along the coast of Norway, as a continuation of the Baltic Current, from Skagerrak to the Barents Sea*".

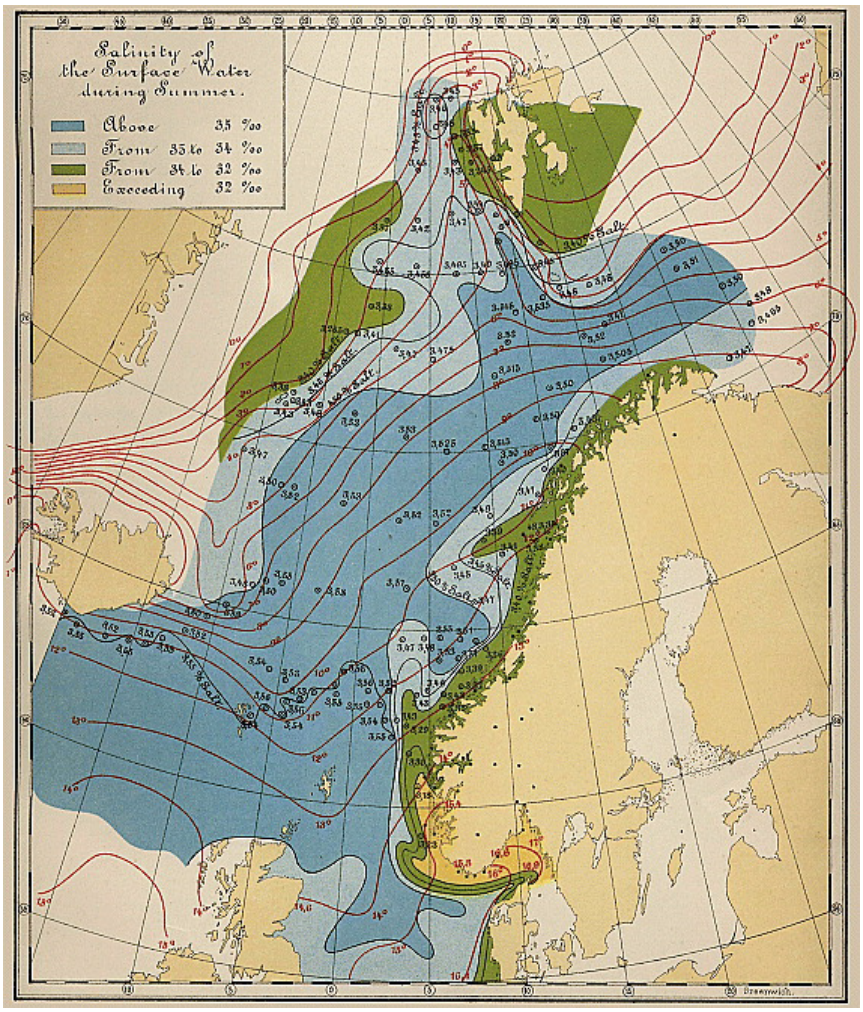

Figure 1: The Norwegian Coastal Water, marked with yellow and green, as illustrated by Hjort and Gran (1899).

Nearly eighty percent of the Norwegian population live within 10 km of the coast. This is due to the availability of food and communications. The coastal zone cover an area of about 100.000 km^2 and has for a long time provided a stable food supply from both stationary and migratory fish stocks and has also facilitated communication by safe sailing in protected areas (Sætre, 2007). The coastal water is an important

constituent in the fjords- and coastal areas along the Norwegian coast, and is of great importance for the coastal ecosystems. Primary production takes place here and it serves as the spawning ground for a number of important fish stocks such as cod and herring. Aquaculture of salmon and trout also takes place all along the coastline of Norway. Thus, the coastal water has attributes and qualities that have great significance for recreation, fishing, tourism and other associated commercial activities (Sætre, 2007).

The NCW derives from an extensive outflow of freshwater from the Baltic Sea and river runoff from the Norwegian coast, making the water less saline than offshore waters (Sætre, 2007). The water mass mixes with the North Sea and North Atlantic Water (NAW) as it flow northwards toward the Barents Sea. The salinity within the current gradually increases northward along the coast and its stratification decreases as it mixes (Sætre, 2007). On its way to the Barents Sea, the coastal water will flow in and out of fjords situated along the coast (Aksnes, 2015). The less saline NCW will float on top of the more saline and dense NAW, preventing the NAW from penetrating fjords with shallow sills, allowing the coastal water to fill the entire fjord basin in such fjords (Aksnes et al., 2009).

The NAW and the NCW are the two water masses that dominate off the Norwegian coast (Sætre, 2007). The NCW is characterized by a salinity < 34.5 and forms a wedge between the coastline and the NAW which is characterized by salinity greater than 35 (Sætre, 2007).

Freshwater supply, tides, winds, inflow of Atlantic water and bottom topography influence the movements and properties of the NCW (Sætre, 2007). The NCC is driven by its density gradients, which mainly are determined by the salinity distribution. However, a considerable part of the current speed is also driven by the gradients in sea levels (IMR, 2013). The typical speeds are 20-50 cm/s, but speeds exceeding 100 cm/s may also take place (Sætre, 2007).

As already mentioned (section 1.1.), freshwater contain dissolved organic substances that absorb light. Such substances may have both marine and terrestrial origin and are often referred to as chromophoric dissolved organic matter (CDOM).

1.3 CDOM

Microbes usually break down most organic matter within a short period of time to carbon dioxide (CO_2) and inorganic forms of nitrogen, sulphur and phosphorus. During the microbial degradation process a complex group of compounds is formed, previously often referred to as "humic substances" (Kirk, 2011). However, in recent papers the acronym CDOM is most commonly used and stands for either *coloured dissolved organic matter*, or *chromophoric dissolved organic matter* (Kirk, 2011), this is the fraction of DOM that interacts with solar irradiance (Nelson and Siegel, 2013). These substances are suggested to be polymers consisting of aromatic rings that are joined together by long-chain alkyl structures to form a flexible network (Schulten et al., 1991). Furthermore, it is from these substances that the yellow-coloured dissolved organic matter in inland – and marine waters is derived (Kirk, 2011).

CDOM are yellow to brown in colour and classified on the basis of their solubility behaviour, which puts them into three main fractions; Humin, humic acid and fulvic acid (Kirk, 2011). All three fractions are however chemically very similar and differ mainly in molecular weight. Humic and fulvic acids constitute an important group of organic compounds in soils and natural waters. Fulvic acid from river inflow is the main contributor to the yellow colour in the sea (Kirk, 2011). Although the specific absorption (per unit mass, at 440 nm) of marine fulvic acid is much lower than that of marine humic acid (Carder et al., 1989), this is made up for by the much higher concentration of fulvic acid. In this way the two forms of dissolved humic material make similar contributions to the absorption of light in the ocean (Kirk, 2011), particularly in the coastal transition zone (Nelson and Siegel, 2013). CDOM in freshwaters, originating from soil humic material and terrestrial and aquatic plants, accounts for 30 to 50 % of the dissolved organic carbon (DOC) in surface waters (Thurman et al., 1982).

The colour of CDOM is due to the presence of multiple double bounds (Kirk, 2011), and the dissolved yellow material has previously been referred to as 'yellow substance', 'gelbstoff', 'yellow organic acids', 'humolimnic acid', 'fulvic acid' etc. Kirk (2011) suggested the word 'gilvin', a noun derived from the Latin adjectives *gilvus* meaning pale yellow. The word gilvin is defined as a general term to be applied

to all or any of these soluble yellow substances which occur in natural waters, regardless of their chemical nature, at a concentration sufficient to contribute significantly to the attenuation of photosynthetically active radiation (PAR) (Kirk, 2011).

CDOM associated with freshwater runoff have long been identified as an important contributor to the light attenuation of coastal waters (Sverdrup et al., 1942). CDOM absorbs a substantial fraction of PAR in lakes (Thrane et al., 2014) and has an absorption spectrum rising exponentially into the blue in surface waters (Kirk, 2011). In open ocean waters, CDOM also dominate the light absorption, and nearly 50 % of the total light absorption at 400 nm is due to CDOM (Nelson and Siegel, 2013). A convenient parameter, of which the concentration of CDOM may be indicated, is the absorption coefficient at 440 nm, g_{440} (soluble colour). This wavelength is chosen because it corresponds approximately to the mid-point of the blue waveband peak that most classes of algae have in their photosynthetic action spectrum (Kirk, 2011).

CDOM show strong correlation with the DOC concentration (Tranvik, 1990; Thrane et al., 2014), especially shown in studies conducted in coastal waters (Mannino et al., 2008). This is because the molecules constituting DOC have strong chromophoric properties (Leenheer and Croue, 2003). The concentration of DOC in boreal lakes has increased over the past decades in many regions (Evans et al., 2005). As CDOM and DOC have strong light-absorbing properties, a future scenario with higher concentration will likely result in reduced light availability, and the depth of the euphotic zone will decrease with an increased concentration of CDOM, and consequently lower the gross primary production (Thrane et al., 2014). The negative effects of CDOM and DOC concentration on primary productivity in boreal lakes have been explained by shading which leads to reduced euphotic depth and faster attenuation of blue light in the water column (Thrane et al., 2014).

Marine waters generally contain much less CDOM than inland waters, decreasing with distance from land (Kirk, 2011). Monahan and Pybus (1978) found that in regions with major river discharge off the west coast of Ireland, the concentration of soluble humic substances diminishes linearly with increasing salinity, indicating that most of the humic substances originate in the rivers. The NAW has a low

concentration of such substances and therefore absorb light to a much lower extent than the fresher coastal water, making the NCW darker than the NAW (Aksnes, 2015).

1.4 Signs of coastal water darkening

The term "coastal water darkening" is not very established, and is to my knowledge used for the first time by Aksnes et al. (2009). Such "darkening" has been observed by means of Secchi observations in several regions, including the Baltic Sea (Fleming-Lehtinen and Laamanen, 2012; Sanden and Håkansson, 1996) and the North Sea (Dupont and Aksnes, 2013). An increasing trend in vegetation cover has been observed (Larsen et al., 2011b; Finstad et al., 2016), which potentially may lead to higher loads of CDOM in rivers (Larsen et al., 2011a). As CDOM absorbs light, increased CDOM concentration together with increased algal-concentrations will cause darkening of a water mass.

One of the climate predictions for our latitude is that future precipitation will continue to increase, as it has over the last 40 years in Norway (Sorteberg, 2014), potentially making the coastal water fresher. Evidence suggests that the basin water of some fjords containing NCW have darkened as a result of NCW freshening over the period 1935-2007 (Aksnes et al., 2009). This freshening, which has been linked to increased precipitation and runoff in Northern Europe and increased westerly winds associated with a high North Atlantic Oscillation (NAO) (Sætre, 2007), may have contributed to a long-term increase in the light attenuation of the NCW (Aksnes et al., 2009). Also, a large increase in CDOM concentration is predicted in Scandinavian freshwater sources in the coming years (Larsen et al., 2011a), which ultimately will end up in the Baltic and the North Sea affecting the NCW (Dupont and Aksnes, 2013). Due to increased DOC or CDOM load in streams and lakes, several studies have suggested a browning of freshwaters, particularly boreal freshwaters around the North Sea, and of waters entering coastal areas in general (Evans et al., 2005; Roulet and Moore, 2006). Moreover, the browning has also been attributed to the recent reduction in sulphate deposition during the last couple of decades, affecting the export of DOC by altering the solubility of organic matter (Finstad et al., 2016).

Riverine and coastal waters are known to attenuate light more than oceanic water does (Kirk, 2011). This is a result of higher concentrations of dissolved matter, including dissolved organic matter (DOM) and CDOM within the freshwater component of coastal water (Aksnes et al., 2009; Frigstad et al., 2013). Terrestrial CDOM that is transported with freshwater gets diluted when it mixes with seawater in the coastal zone, leading to a decrease in CDOM absorption. Absorption of light is therefore inversely related to salinity (Kowalczuk et al., 2005; Højerslev et al., 1996; Stedmon and Markager, 2003). Thus, salinity appear to be an efficient proxy for light absorption, attenuation, and thereby also for Secchi depth (Dupont and Aksnes, 2013; Aksnes, 2015). If increased precipitation and runoff, owing to global climate change, have an effect on salinity (Greene et al., 2008), we additionally expect changes within the coastal light regimes with potential ecosystem implications (Aksnes et al., 2009).

Light absorption has also been suggested to increase with oxygen depletion (Sørnes and Aksnes, 2006). This can be of importance as decreased dissolved oxygen in subsurface waters follows eutrophication and has resulted in anoxic conditions in coastal areas and shelf regions world-wide, including coastal regions of Scandinavia (Aksnes et al., 2009; Aure et al., 1996). Aksnes et al. (2009) suggested that the NCW freshening has been associated with a water column darkening that has been most pronounced at coastal locations where NCW penetrate to mesopelagic depths.

Water column light attenuation is a critical ecosystem variable due to its effect on primary production, but also because different organisms are sensitive to light. Proxies of CDOM and its light attenuation, e.g. salinity and oxygen are therefore found to be useful in analyses of environmental changes (Aksnes, 2015).

1.5 The aims of this study

The objective of this thesis is to provide a better theoretical foundation for assessing the causes of ecosystem changes in fjords and coastal areas. This is facilitated by sensitivity analyses of how NCW euphotic zone properties respond to expected changes in light absorption associated with increasing input of dissolved terrestrial matter, i.e. CDOM. The euphotic zone properties will be characterized by some indicators such as the euphotic depth, Secchi depth and nutricline depth, along with the vertical distribution of nutrient and phytoplankton concentration.

Similar to the study of Urtizberea et al. (2013) I have applied the simulation model of Huisman et al. (2006) for simulations of how the euphotic zone properties are affected by changes in light attenuation. The light attenuation in my study is aimed at reflecting the NCW during a summer situation in the past, present and for the future.

Observations and information from three coastal locations retrieved from literature (Erga, 1989a; Erga, 1989b; Erga and Skjoldal, 1990; Paasche and Erga, 1988) will be used as the basis for adapting the simulation model of Huisman et al. (2006) to the NCW. Further, time series of Secchi depth (Fleming-Lehtinen and Laamanen, 2012) and coastal station data from IMRs fixed hydrographic stations have been used as a proxy for changes in light attenuation and stratification, respectively.

2 MATERIALS AND METHODS

In brief, sensitivity analyses with the Huisman et al. (2006) model are to be conducted on how euphotic zone properties of the NCW are expected to respond to increased light absorption associated with an increasing supply of terrestrial organic matter.

2.1 Data

From literature it has been possible to collect data about the vertical distribution of some components including nutrients, phytoplankton, salinity and temperature from three fjord locations along the South Norway. These have been used to see to what degree the simulation model of Huisman et al. (2006) reproduce the variety found in observed vertical structures. Also, time series from IMRs fixed hydrographic stations, at Lista and Sognesjøen representing two coastal stations, served as a proxy for changes in stratification. Secchi depth studies (Fleming-Lehtinen and Laamanen, 2012) have been used as a proxy for changes in light attenuation. In order to run the Huisman et al. (2006) simulation model input values of background attenuation (K_{bg}) and turbulent diffusivity (κ) are required, and have been obtained from salinity and stratification, respectively (see section 2.3.1).

2.1.1 Data from three fjord locations

Fjords and polls are characterized by having stratified water-masses, especially during the summer (Aksnes et al., 1985). Some previous studies involving Norwegian waters have been included to see how well the idealized model of Huisman et al. 2006 reproduce the main features of observed summertime nutrient-and phytoplankton vertical distributions. These studies are based on data collected in Boknafjorden (Erga, 1989a; Erga, 1989b), Lindåspollene (Erga and Skjoldal, 1990), and Oslofjorden (Paasche and Erga, 1988) (Fig. 2).

These studies were chosen as they contain measurements of nutrients, phytoplankton, salinity and temperature sampled in the vertical during summer. In fact, relatively few

studies provide vertical structure of nutrients, phytoplankton, salinity and temperature in Norwegian coastal waters during summer. In this situation an "equilibrium" situation with a deep chlorophyll maximum is expected. Furthermore, the three localities are distributed at different locations along the coast of southern Norway. In addition, the same researcher (Svein Rune Erga) has been involved in all the studies, which may have been an advantage in respect to methodology.

Figure 2. Map over the three fjord locations (Lindåspollene, Boknafjorden and Oslofjorden) marked in blue, including two of IMRs fixed hydrographic stations (Sognesjøen and Lista) marked in red.

Site description

Lindåspollene is a land-locked fjord situated in Nordhordland, western Norway (Erga and Skjoldal, 1990). The fjord has restricted water exchange, as only a narrow entrance connects it with the outside fjord system (Aksnes and Lie, 1990).

Boknafjorden is a deep-silled fjord of southwestern Norway. It is located in Rogaland County, and constitutes the outer part of the Ryfylke fjords. The fjord is wide and deep, with a maximum depth of about 620 m. To the west, there is a sill of about 200 m connecting the fjord water to adjacent coastal waters (Erga, 1989a).

Oslofjorden, a brackish-marine fjord in southeastern Norway, is part of the Skagerrak strait, connecting the North Sea and the Kattegat sea area. It is divided into the inner and outer Oslofjord. The inner Oslofjord is a sill fjord, with a sill of about 19.5 m located in the narrow entrance to the fjord at Drøbak, while the outer Oslofjord connects the Oslofjord to the Skagerrak (Molvær et al., 2007). The Oslofjord has served as a recipient of sewage and to a lesser degree industry (Paasche and Erga, 1988; Molvær et al., 2007).

Data collection

The data, i.e. temperature, salinity, nutrients (nitrate), and phytoplankton concentration (Chl a) were read manually from figures in the published studies. Samples collected in June-July were chosen to represent the summer situation. Observations made the same day at the same location, but at different hours were averaged to present that day. For each location the measurements were then averaged to represent the summer period for that particular location. In the studies of Boknafjorden and Lindåspollene, most of the samples were taken from various light depths within the euphotic zone. This allowed me to estimate the euphotic depth, corresponding to 1% of the surface irradiance (Kirk, 2011). Boknafjorden had few measurements of nitrate (NO_3^-), thus orthophosphate (PO_4) was used instead. These values were converted to nitrate as this was the currency of the simulation model, using a NO_3:PO_4 ratio of ~5 based on the measurements of nutrients in the euphotic

zone, and a ratio of ~15 based on measurements of nutrients from the bottom of the euphotic zone and down to 40 m.

2.1.2 IMRs fixed hydrographic stations

Jens Eggvin of the Institute of Marine Research (IMR) initiated a network of fixed oceanographic observation stations along the coast in 1935, which were set to monitor the temperature and salinity of the coastal water. This monitoring is still in progress and represents the longest continuous oceanographic time series in the world (Sætre, 2007). The time series (http://www.imr.no/forskning/forskningsdata/stasjoner/) provided information on long-term changes in salinity and temperature. Salinity changes were applied as a proxy for background attenuation, while changes in both temperature and salinity affect the density stratification and were applied as a proxy for the vertical turbulent diffusivity (see section 2.3.1). Measurements of temperature and salinity from the two stations, Lista and Sognesjøen (Fig. 2), were used in the present study.

2.1.3 Secchi depth observations

Secchi depth observations have been collected in the Baltic- and North Sea since 1903. There are more than 40 000 observations of Secchi depth during this period, compiled by Aarup (2002), which result in an extensive long-term dataset (Dupont and Aksnes, 2013; Fleming-Lehtinen and Laamanen, 2012). The data set provides information of the changes in the light environment, and indicates a decreased water transparency in the Baltic Sea (Fleming-Lehtinen and Laamanen, 2012; Sanden and Håkansson, 1996) and in the North Sea (Dupont and Aksnes, 2013) during the last hundred years.

2.2 Simulation model

2.2.1 The simulation model of Huisman et al. (2006)

The idealized simulation model of Huisman et al. (2006) was applied to simulate the vertical distribution of nutrients and phytoplankton. The dynamics of the phytoplankton population (P, cells m^{-3}) and the nutrient concentration (N, mmol N m^{-3}) in the water column are given as a function of time (t) and depth (z) (Huisman et al., 2006):

$$\frac{\partial P}{\partial t} = \mu(N,I)P - mP - v\frac{\partial P}{\partial Z} + \kappa\frac{\partial^2 P}{\partial z^2} \qquad (1)$$

$$\frac{\partial N}{\partial t} = -\alpha\mu(N,I)P + \varepsilon\alpha mP + \kappa\frac{\partial^2 N}{\partial z^2} \qquad (2)$$

where m (s^{-1}) is the specific loss rate (mortality) of the phytoplankton, v (m s^{-1}) is the phytoplankton sinking velocity, κ (m^2 s^{-1}) is the vertical turbulent diffusivity, α is the nitrogen content of the phytoplankton, ε is the proportion of nitrogen in dead phytoplankton that is instantaneously recycled back to the nutrient pool, and $\mu\ (N, I)$ is the specific growth rate of phytoplankton.

As both light and nutrients can be limiting factors, modellers often assume that the specific growth rate of phytoplankton, $\mu(N,I)$, comprises the product of two independent functions of light and nutrient concentration (Sarmiento and Gruber, 2006): $\mu(N,I) = \mu(N) \cdot \mu(I)$. Huisman et al. 2006 assumed that the specific growth rate of the phytoplankton followed the Monod equation, and was determined by the resource that was most limiting according to Von Liebig's law of the minimum. Hence, the formulation of *μ(N,I)* is the specific growth rate of the phytoplankton as an increasing saturating function of nitrate availability N and light intensity I (PAR):

$$\boldsymbol{\mu(N,I) = \mu_{max} min\,(\frac{N}{H_n+N}, \frac{I}{H_i+I})} \qquad (3)$$

where μ_{max} is the maximum specific growth rate, H_n and H_i are the half-saturation constants i.e. the concentration at which the growth rate is half its maximum value for nutrient-limited and light-limited growth respectively, and *min* denotes the minimum function.

Light intensity, *I*, supplied from above decreases exponentially with depth according to Lambert-Beer's Law:

$$\boldsymbol{I = I_{in} exp\,(-K_{bg} z - k_p \int_0^z P(t,\sigma) d\sigma)} \qquad (4)$$

where I_{in} is the incident light intensity, K_{bg} is the background light attenuation of the water column, k_p is the specific light absorption coefficient of the phytoplankton, and σ is an integration variable accounting for the non-uniform phytoplankton population density distribution with depth. The total light attenuation in the model comprises K_{bg} and the attenuation from phytoplankton. In the present study the background attenuation (K_{bg}) represents CDOM-attenuation, as for Urtizberea et al. (2013).

Huisman et al. (2006) parameterized their model for clear ocean water (see Table 1 in Supplementary Information, Huisman et al., 2006), and were simulated at different intensities of vertical mixing. To show an example of a Huisman et al. (2006) model simulation, I ran the simulation model using low levels of mixing ($\kappa = 1.2\times10^{-5}$ m^2 s^{-1}) and background light attenuation ($K_{bg} = 0.045$ m^{-1}) (Fig. 3).

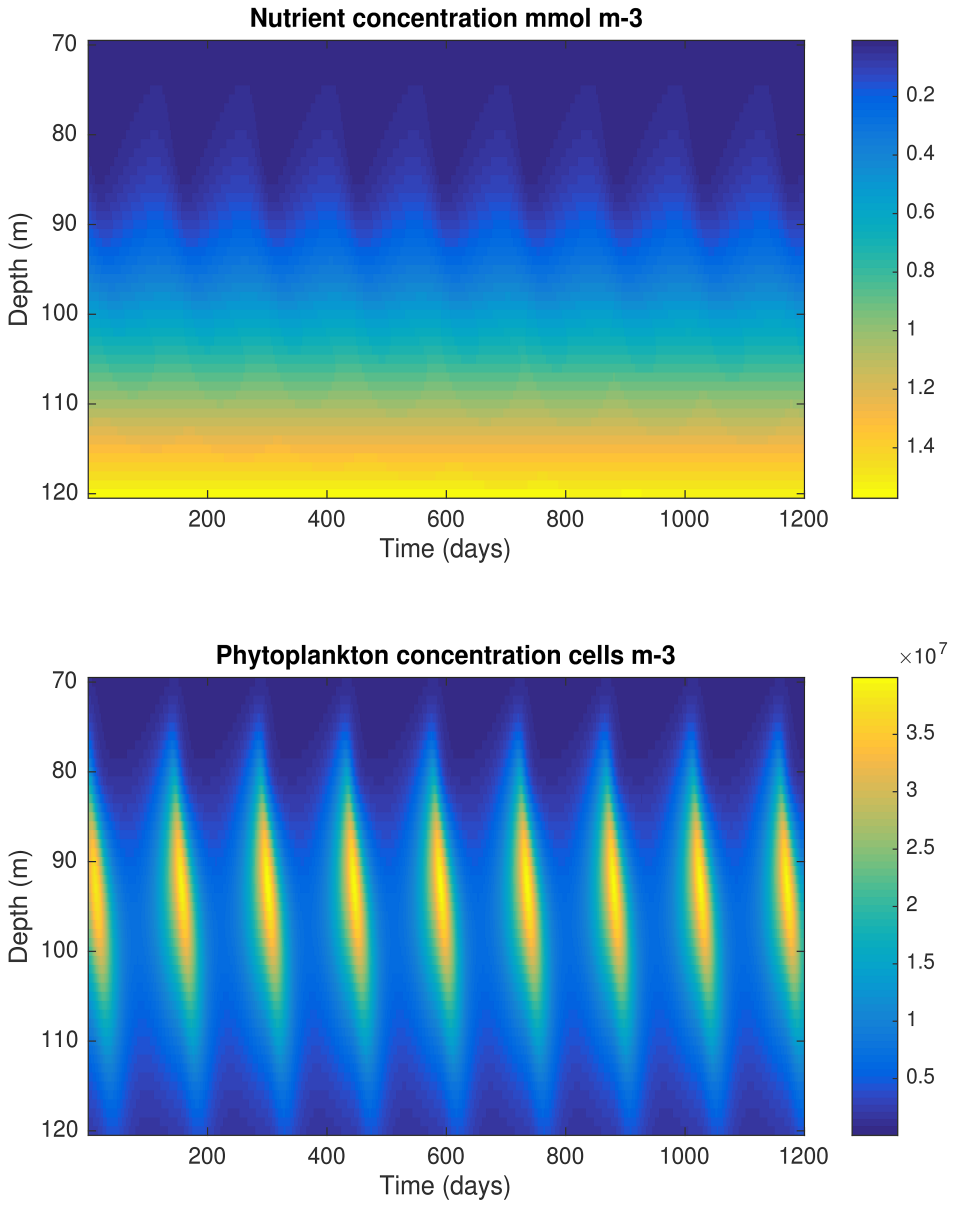

Figure 3. Huisman et al. (2006) demonstrated that low levels of mixing, i.e. a turbulent diffusivity coefficient (κ) lower than 5.0 $\times 10^{-5}$ $m^2 s^{-1}$, would generate oscillations and chaos in the oceanic deep chlorophyll maximum (DMC). Further, for values over this threshold the model was predicted to converge towards a stable equilibrium at which the downward flux of consumed nutrients was equal to the upward flux of new nutrient. To show an example of a Huisman et al (2006) model simulation, I ran the model using low levels of mixing and background attenuation. This example demonstrates that large-amplitude oscillations in the DCM may be observed for $\kappa = 1.2 \times 10^{-5}$ $m^2 s^{-1}$ and $K_{bg} = 0.045$ m^{-1}.

2.2.2 Model modifications

From clear ocean water to coastal water

Huisman et al. (2006) parameterized (as already mentioned) their model for oligotrophic subtropical waters. In such waters, the clear water attenuation coefficient (K_w) is often set to a value close to 0.04 m^{-1} for PAR in simulation models (Sarmiento and Gruber, 2006; Aksnes, 2015). Huisman et al. (2006) used a value of 0.045 m^{-1} for the background turbidity. The specific light absorption coefficient of the phytoplankton (k_p) in Eq. (4), is a subject to large variation in nature (Bricaud et al., 1995). Hence, since coastal waters tend to be more eutrophic, a modification of the linear term k_pP from Eq. (4) in the Huisman et al. (2006) model was done.

Morel and Maritorena (2001) proposed that the chlorophyll contribution to the light attenuation for downwelling irradiance do not behave linearly. They assumed that the attenuation coefficient, K, could be considered as the sum of K_w and K_{bio} (here, corresponding to K_pP from Eq. 4), a term merging the contributors of all biogenic components (phytoplankton), so that its spectral value is:

$$\boldsymbol{K(\lambda) = K_w(\lambda) + K_{bio}(\lambda)} \qquad (5)$$

Then $K_{bio}(\lambda)$ at each wavelength is related to chlorophyll (Chl) and its coefficients can be expressed as power laws (Morel and Maritorena, 2001):

$$\boldsymbol{K_{bio}(\lambda) = \chi(\lambda)(Chl)^{e(\lambda)}} \qquad (6)$$

The attenuation of light is wavelength-dependent. Note that in the model of Huisman et al. (2006) light energy is approximated by the photosynthetic active radiation (PAR). In the present study, a wavelength of 440 nm was chosen because of its correspondence to the mid-point of the blue waveband peak that most classes of algae have in their photosynthetic action spectrum (Kirk, 2011). Further, the proxy model for background attenuation (see Eq. 8) (Aksnes, 2015) is also approximated for 440

nm. The spectral values for χ (λ) and e (λ) at a wavelength of 440 nm are 0.11 and 0.67, respectively (given in Table 2 of Morel and Maritorena, 2001), so that the effect of chlorophyll on K at a wavelength of 440 nm corresponds to: $K_{bio} = 0.11(Chl)^{0.67}$ where (*Chl*) is the chlorophyll concentration in mg m^{-3}.

Conversion of units

The phytoplankton concentration (P) was given in units of cell m^{-3} in Huisman et al. (2006), while P in this study is given in unit mmol N m^{-3}. Hence, the unit of (*Chl*) in Eq. (6) was converted from chlorophyll mg m^{-3} to mmol N m^{-3} using a carbon-to-chlorophyll ratio of 50, a C:N mole ratio of 117:6, and the atomic weight of carbon, 12 mg mol^{-1} (Sarmiento and Gruber, 2006). Provided that phytoplankton now is expressed in mmol N m^{-3}, Eq. (6) (at a wavelength of 440 nm) becomes:

$$\boldsymbol{K_{bio} = 0.16(P)^{0.67}} \qquad (7)$$

K_{bio} was used to calculate the contribution of phytoplankton to light attenuation. Consequently, the total light attenuation in the model consists of K_{bio} and K_{bg}.

2.3 Variables

This section will present the input parameters, i.e. K_{bg}, κ and N_B (i.e. the fixed nutrient concentration in the last depth cell) used in the simulation model, along with the output parameters that are analysed/presented in this thesis.

2.3.1 Input parameters

Salinity as a proxy for the background attenuation coefficient (K_{bg})

Attenuation of light in the water column is due to absorption and scattering. The total attenuation coefficient for downward irradiance in simulation models is often described as $K = K_w + K_pP + K_x$ (Sarmiento and Gruber, 2006; Urtizberea et al., 2013; Aksnes, 2015), where K_w represents attenuation due to clear water, K_pP the

attenuation due to phytoplankton biomass (where P is the phytoplankton concentration and K_p the specific attenuation coefficient), and K_x the attenuation due to other particulate and dissolved matter, i.e. non-phytoplankton constitutes.

According to Sarmiento and Gruber (2006), K_x is generally ignored in simulation models. However, some ecological modelling studies do include the optical effects, thereby K_x, of constitutes such as CDOM (Aksnes, 2015). Hence, modellers often assign a constant value, K_{bg}, to the background attenuation rather than utilizing two independent measures of K_w and K_x. Here, the background attenuation (K_{bg}) is used to represent the CDOM contribution to the light absorption in the study range (Urtizberea et al., 2013).

It has been suggested that K_{bg} might contribute more to the total light attenuation than phytoplankton in coastal waters (Urtizberea et al., 2013). There is a strong inverse relationship between salinity and CDOM absorption (Kowalczuk et al., 2003), and since lower salinity generally means higher CDOM concentrations, and thereby higher light attenuation, salinity might serve as a proxy for the background light attenuation (Urtizberea et al., 2013).

Aksnes (2015) estimated an empirical model where salinity served as a proxy for the non-phytoplankton NCW light attenuation, i.e. the background attenuation (K_{bg}). It was assumed that the water samples of NCW were a mixture of two end-member water masses; oceanic water (NAW) and freshwater (FW), and also that K_{bg} was determined by the mixing ratio of the two water masses and the respective non-phytoplankton attenuations, K_{NAW} and K_{FW}, so that:

$$\boldsymbol{K_{bg} = K_{FW} + k_1 Sal} \qquad (8)$$

Statistical effects of salinity on K at 440 nm estimated with multiple regression analysis (see Table 3 in Aksnes, 2015) provided a K_{FW} =1.47 ± 0.05 (m^{-1}), which is the estimated attenuation of freshwater draining to NCW, and a k_1 = - 0.041 ± 0.003 m^{-1} $(PSU)^{-1}$, which is an estimate of how much K_{FW} decreases for an increase of one

PSU (and a K_{NAW} = 0.03 m^{-1}). Consequently, salinity may serve as a proxy for the background attenuation according to:

$$\boldsymbol{K_{bg} = 1.47 - 0.041 \cdot Sal} \qquad (9)$$

In the simulations of the vertical structure at the three fjord locations (Lindåspollene, Boknafjorden and Oslofjorden), I applied the average salinity between the surface and the depth of the chlorophyll maximum at each location to calculate K_{bg} from Eq. (9).

Turbulent diffusivity

In addition to K_{bg}, the turbulent diffusivity (κ) is needed to run the Huisman et al. (2006) simulation model.

Vertical density gradients in the ocean are influenced by gravity, that is the buoyancy force will act on a moving particle to either stabilise ($dr/dz < 0$) or destabilise ($dr/dz > 0$) the water column (Monin, 1990). The stratification can be expressed by the buoyancy frequency (N), also called stability frequency or Brunt-Väisälä frequency (s^{-1}) (Eq. 11).

Turbulent diffusion or eddy diffusion is due to random fluctuation in a current velocity. The turbulent diffusion coefficient (κ) is influenced both by the dissipation rate of turbulent kinetic energy (e) and the buoyancy frequency (N) as in the empirical formulation by Denman and Gargett (1983) :

$$\boldsymbol{\kappa = 0.25 e N^{-2}} \qquad (10)$$

$$\boldsymbol{N^2 = (g/r)\,(dr/dz)} \qquad (11)$$

Where *g* is the acceleration due to gravity, *r* is the density of water, and *dr/dz* is the vertical density gradient.

According to Eq. (10) and (11), κ is a function of the dissipation rate (e) and the Buoyancy frequency (N). I used the calculated buoyancy frequency as a proxy for the turbulent diffusivities in the simulations of vertical structure at the three fjord locations, and for past and future scenario simulations of NCW euphotic zone properties at two coastal stations by assuming a constant wind speed/dissipation rate (see below).

Density was not reported in the studies of Lindåspollene, Boknafjorden and Oslofjorden. To enable calculation of the buoyancy frequency, the density was computed from the state variables, salinity and temperature, using an online "water density calculator" (http://www.csgnetwork.com/h2odenscalc.html). As the study from Oslofjorden lacked measurements of temperature (except for the surface), the summer temperature depth profile for Lindåspollene was used also for this location. Presumably, the density calculation was not seriously affected by this approximation since vertical differences in salinity had by far the largest effect on density.

For past and future scenario simulations, differences in density at a depth of 10 and 50 m from two coastal stations (see section 2.1.2) were used to approximate N and consequently the turbulent diffusivity for the past and present. Further, density extrapolation allowed me to approximate a turbulent diffusivity for the future.

Dissipation rate for turbulent kinetic energy

In order to calculate the turbulent diffusivity (κ) (Eq. 10), one also needs to assume a dissipation rate for turbulent kinetic energy (e). In a simulation study of Lindåspollene, Aksnes and Lie (1990) assumed, based on Denman and Gargett (1983), that values of *e* could be calculated from the actual wind strength (W, ms^{-1}) using the following equation:

$$e_A = a_1 W^3 + a_2 \qquad (12)$$

where a_1 and a_2 are constants, namely 4.9×10^{-9} m^{-1} and 4.23×10^{-8} m^2s^{-3} respectively (given in Table 4 of Aksnes and Lie, 1990).

In this study I also used Eq. (12) to approximate the dissipation rate of turbulent kinetic energy (e) for a summer situation in Lindåspollene where winds usually are weak and assumed to be 3 m/s here. Further, I assumed the same *e* for simulation of the two other fjord locations and for the past and future simulated scenarios, and could from this utilize the buoyancy frequency to find a level of turbulent diffusivity.

Nutrient concentration at the deepest cell of the water column (N_B)

Nutrients (nitrate) were replenished from below with a fixed nutrient concentration (N_B) in the deepest cell of the water column, i.e. at 50 m. N_B was assumed to be 15 mmol N m^{-3} for the simulation, except for the simulation of Oslofjorden.

2.3.2 Simulated euphotic properties

Simulated vertical distributions of nitrate and phytoplankton and associated euphotic zone properties were analysed and presented. These properties include the euphotic depth, Secchi depth and the nutricline depth (explained below), along with the surface integrated biomass of phytoplankton (Bi) and primary production per hour (Pi) (both expressed in nitrogen), and the sum of nutrients in the upper 20 m of the water column (SumN).

Euphotic depth

Euphotic zone depth (Z_E) was taken as the depth where only 1 % of the surface photosynthetically available radiation (PAR) remains (Kirk, 2011). This depth serves as a measure of water clarity, which is an important parameter regarding ecosystems (Lee et al., 2007). It is commonly used to represent the "compensation depth" where photosynthesis balances respiration, i.e. no net phytoplankton growth at this depth/light (Kaiser et al., 2011).

Secchi depth

The Secchi disc, a white disc that is usually 30-cm in diameter, is one of the few early hydrological measuring devices still in use (Fleming-Lehtinen and Laamanen, 2012). The technique, in which the disc is lowered vertically into the water until it disappears from sight, was created by Angelo Secchi in 1865 (Preisendorfer, 1986). Because of the method's simplicity, Secchi depth readings have been used extensively (Sanden and Håkansson, 1996).

Kirk (2011) proposed that the relation between Secchi depth and the light attenuation coefficient (K) could be approximated as following:

$$\boldsymbol{S = \frac{1.44}{K}} \qquad (13)$$

where S is the Secchi depth. I used this expression to calculate the simulated Secchi depth where K represented the simulated total light attenuation coefficient between the surface and the Secchi depth.

Nutricline depth

In most regions, nitrate is often exhausted close to the ocean surface by phytoplankton utilization and increases with depth displaying a strong vertical gradient, here referred to as the nutricline (Omand and Mahadevan, 2015). The transport of nitrate into the euphotic zone is an important regulator of primary production, and this transport is associated with the depth and the steepness of the nutricline (Aksnes et al., 2007). I have used the first depth where the nitrate concentration was approximately equal to 1 mmol N m^{-3} to define the nutricline depth (Z_N) (Lavigne et al., 2013; Pasqueron de Fommervault et al., 2015).

2.4 Simulated scenarios

Increased light absorption associated with an increasing input of CDOM are expected in the NCW (Larsen et al., 2011a), and may consequently also affect the NCW euphotic zone properties. In the present study the background attenuation (K_{bg}) represent CDOM-attenuation. After I investigated whether the Huisman et al. (2006) model was able to reproduce main vertical features of the three fjord locations, the vertical distributions of nitrate and phytoplankton, and associated euphotic zone properties of the NCW during an idealized summer situation at two coastal stations were simulated for the past, present and for the future.

2.4.1 Present

The "present" scenario was defined as the year 2010 on the grounds that the salinity proxy for K_{bg} (Eq. 9) was based on surveys completed in 2010 (Aksnes, 2015).

2.4.2 Past

Time-series of temperature and salinity goes all the way back to 1935 and 1942 at station Sognesjøen and Lista, respectively. In that case, the "past" scenario was defined as the year 1935 and 1942 for Sognesjøen and Lista, respectively.

Secchi depth is a useful proxy for distinguishing long-term changes in water clarity of oceanic and coastal ecosystems (Sanden and Håkansson, 1996; Dupont and Aksnes, 2013). Although it may be best known as an indirect measure of phytoplankton biomass, productivity and eutrophication, it is ultimately a proxy of optical properties (Preisendorfer, 1986):

$$\boldsymbol{S} = \frac{\boldsymbol{\Gamma}}{\boldsymbol{K}+\boldsymbol{c}} \qquad (14)$$

where K (m^{-1}) is the attenuation coefficient of downwelling irradiance, c (m^{-1}) the beam attenuation coefficient, and Γ is termed the coupling constant, whose value typically is 8-9 (Kirk, 2011).

A change in Secchi depth is commonly reported as the change in metres (Dupont and Aksnes, 2013), but from Eq. (14) we see that Secchi depth relates inversely to the attenuation coefficient. There is much evidence that the product, $K \cdot S$, in reality is not constant, especially in inland waters, as Secchi depth is particularly sensitive to turbidity (Kirk, 2011). Since K and c relate inversely to Secchi depth (Eq. 14), changes in the reciprocal Secchi depth may be of interest from an ecological as well as an optical point of view (Dupont and Aksnes, 2013). Further, the reciprocal Secchi depth, i.e. 1/S, is proportional to the sum of the beam attenuation coefficient, c, and the vertical attenuation coefficient, K as can be seen from Eq. (14).

For the past scenario, I assumed that K changes in proportion to c + K, so that an observed change in 1/S is taken as the relative (not absolute) change in K. The observed change in the reciprocal Secchi depth of the Baltic Sea was used as a proxy for a change in the background attenuation of the freshwater draining to the Baltic Sea and the NCW.

Fleming-Lehtinen and Laamanen (2012) reported shoaling rates on the range 0.01-0.04 m y^{-1} in different sub-regions of the Baltic Sea. Their observations were used to calculate the percentage change in reciprocal Secchi depth between two periods: 1935-1939 and 2005-2009, for each location in Table 1 and then averaged to present the change that was assumed in the past scenario. From previous studies with respect to CDOM absorption and conservative mixing, three important pools of dissolved organic matter exist, including the Baltic Sea, North Sea and German Bight, where conservative mixing of these can explain most of the spatial and temporal in concentration and characteristic of CDOM (Højerslev et al., 1996; Stedmon et al., 2010). Fleming-Lehtinen and Laamanen (2012) also included the Bothnian Bay, Bothnian Sea and the Gulf of Finland in their study. However, with respect to conservative mixing, these three sub-regions deviate from the conservative mixing line (See Figs. 5 and 6 in Højerslev et al., 1996), and are therefore excluded. Such deviation indicate the presence of CDOM sources or sinks, which will cause the inverse linear relationship between terrestrial CDOM and salinity to deviate upward or downward, respectively (del Vecchio and Blough, 2006).

Table 1: Secchi depth observations in different sub-basin of the Baltic Sea (the Bothnian Bay, the Bothnian Sea and the Gulf of Finland are excluded) during two five-year periods: 1935-1939 and 2005-2009 (See Table 1 Fleming-Lehtinen and Laamanen, 2012). The differences in Secchi depth means (in metres), the average difference in metres per year (Secchi shoaling rate) and the reciprocal Secchi depth (1/S) are included. % (1/S) expresses the reciprocal secchi depth in an early period as a percentage of the reciprocal Secchi depth in a late period.

Sub-region	**Years**	**Mean (m)**	**Secchi shoaling rate (m y^{-1})**	**1/S**	**% (1/S)**
Northern Baltic Proper	1935-1939	8.2	0.040	0.122	
	2005-2009	5.4		0.185	66
Gulf of Riga	1935-1939	3.9	0.012	0.254	
	2005-2009	3.1		0.323	79
Eastern Gotland Basin	1935-1939	7.6	0.020	0.132	
	2005-2009	6.2		0.161	82
Western Gotland Basin	1935-1939	7.4	0.020	0.135	
	2005-2009	6.0		0.167	81
Bornholm Basin	1935-1939	8.1	0.022	0.123	
	2005-2009	6.6		0.152	81
Arkona Sea	1935-1939	8.1	0.012	0.123	
	2005-2009	7.3		0.137	90

It can be seen from Table 1 that reciprocal Secchi depth in the early period (1935–1939) was on average 80 % of that in the late period. With the assumption that the non-chlorophyll light attenuation of the freshwater source (K_{FW}) in Eq. (8) has changed in proportion to the total percentage change in reciprocal Secchi depth, i.e. 80 %, of the relatively fresh Baltic sea (Fleming-Lehtinen and Laamanen, 2012), I could approximate a change in K_{FW} (from a K_{FW} =1.47 m^{-1} representing the present situation, Eq. 9). I made the assumption that attenuation due to CDOM is mixed conservatively and estimated:

$$\boldsymbol{k_1} = \frac{\boldsymbol{K_{NAW} - K_{FW}}}{\mathbf{35.2}} \qquad (15)$$

So that k_1 from Eq. (8) was approximated on the basis of the K_{FW} now representing the early period (1935–1939), K_{FW} = 1.17 m^{-1} (i.e. 80% of the 1.47 m^{-1}). K_{NAW} for the

early period was assumed equal to that of the present, i.e. K_{NAW} = 0.03 m^{-1}. From this, a proxy for background attenuation for the past scenario could be obtained:

$$\boldsymbol{K_{bg} = 1.17 - 0.032 \cdot Sal} \quad (16)$$

2.4.3 Future

Larsen et al. (2011) predicted that the median concentration of organic carbon (OC) in a wide number of pristine Norwegian lakes will increase by 65% over the next century. The projected changes of that study were based on model simulations based on future greenhouse gas emissions according to the Intergovernmental Panel in Climate Change (IPCC) Special Report on Emission Scenarios (SRES) B2 scenarios and the general circulation model HadM3H, making projections of climate change out to the year 2100. Particularly northern, boreal regions are expected to experience a strong increase in the OC export from catchments to surface areas (Larsen et al., 2011a; Larsen et al., 2011b).

In the present study, the "future" was separated into two parts; a future 1 scenario, i.e. year 2050, experiencing an increase of organic carbon by 32.5 % (half of that predicted by Larsen et al. 2011a), and a future 2 scenario, i.e. experiencing an increase in OC by 65 %. Further, making the assumption that the non-chlorophyll light attenuation of the freshwater source (K_{FW}) from Eq. (8) changes to the same extent as the organic carbon projections in Larsen et al. (2011a), I increased K_{FW} by the same percentage (from a K_{FW} =1.47 m^{-1} representing the present situation, Eq. 9), i.e. 1.95 and 2.42 m^{-1} for future scenario 1 and 2, respectively. Here, I also make the assumption of conservative mixing (Eq. 15) of organic carbon (and its corresponding light attenuation). From this, keeping K_{NAW} constant (i.e. equal to that of the present scenario, K_{NAW}= 0.03 m^{-1}), a proxy for background attenuation for a future 1 and future 2 scenario could be obtained:

$$\boldsymbol{K_{bg} = 1.95 - 0.055 \cdot Sal} \quad (17)$$

$$\boldsymbol{K_{bg} = 2.42 - 0.068 \cdot Sal} \quad (18)$$

2.5 Applications and data tools

MATLAB and Microsoft Excel were used for analysis and presentation of results.

Data from three coastal locations were collected in Microsoft Excel, and then converted to MATLAB. Data from IMRs fixed hydrographic stations were also assessed using Microsoft Excel, where linear regression analyses were performed.

MATLAB was used for all the simulations using the general simulation model of Huisman et al. (2006) including vertical distributions of nitrate and phytoplankton concentration, and for the predicted variations in euphotic, Secchi and nutricline depth as a function of salinity. The resulting simulated properties of the euphotic zone were compiled in tables and plotted in figures. The MATLAB software used was MATLAB R2015b. The different codes used in the simulations are given in Appendix A.

Except for background light attenuation (K_{bg}), the turbulent diffusivity (κ), the phytoplankton self-shading, and the nitrate concentration in the last depth cell (N_B), I have applied the same parameter values as in Huisman et al. (2006).

Nutrients (nitrate) were replenished from below with a fixed nutrient concentration (N_B) in the deepest cell of the water column. Simulations were made for a 50 m deep water column, with a 1 m resolution and a time step of 300 s. A constant incident light was as in Huisman et al. (2006) applied to achieve a steady state situation. The criterion for steady state was that the annual change in euphotic zone did not exceed 0.1% per year, i.e. $Z_{Echange} < 0.1$ %.

3 RESULTS

The result section is divided into five parts. First I present how the simulation model of Huisman et al. (2006) behaves in relation to observed vertical structures from Lindåspollene (Erga and Skjoldal, 1990), Boknafjorden (Erga, 1989a; Erga, 1989b) and Oslofjorden (Paasche and Erga, 1988). I then go on to assess the temporal trends in temperature and salinity based on observed changes in salinity and temperature from two coastal stations. Further, scenario simulations of NCW euphotic properties based on approximated values of background attenuation are presented, (1) with a constant turbulent diffusivity, (2) using approximated turbulent diffusivities, for the past, present and a future scenario. The last section addresses implication of variation in K_{bg} of NCW as a function of salinity in a gradient from NCW_{24} (i.e. with a salinity of 24) to NAW_{35}.

3.1 Observed and simulated vertical structure in three fjords

Data from three different locations along the southwestern Norwegian coastline were presented to see to what extent the idealized simulation model of Huisman et al. (2006) could reproduce the differences seen in observed vertical structures. In the present study the vertical structure is addressed and no efforts were made to calibrate the simulated phytoplankton concentration with observed concentrations. The observed vertical structure of phytoplankton and nitrate concentration from Lindåspollene, Boknafjorden and Oslofjorden were plotted together (Figs. 4A and 5A, respectively). For comparison, simulated vertical distributions for the same locations, using approximated background attenuations (K_{bg}) and vertical turbulent diffusivities (κ) were also plotted (Figs. 4B and 5B).

Observed vertical structures

The data from the three coastal locations represent a summer situation (Table 2); a season characterized by stratification. Lindåspollene had a mean salinity of 30.5 ‰ down to the chlorophyll top located at a depth of 25 m (Fig 4A). The euphotic depth was situated at approximately 20 m. Measurements of the nutrient concentration

indicated that the surface water in Lindåspollene was nearly depleted of nutrients (nitrate), with a nutricline depth (Z_N) located at about 17 m (Fig. 5A). Boknafjorden had a mean salinity of 29 ‰ down to the chlorophyll top located at a depth of around 17 m (Fig. 4A), which also was the observed euphotic depth. Here, the surface water was also nearly nitrate-depleted, with a nutricline depth located at approximately 19 m (Fig. 5A). Based on data collected in Oslofjorden, a mean salinity of 21 ‰ down to a chlorophyll top located at a depth of 8 m was observed (Fig. 4A). As for the two other locations, the surface water in Oslofjorden was also nitrate-depleted. However, the nitracline depth appeared to be located much shallower here than for the two other fjords, at a depth of 4.5 m (Fig. 5A).

Values from Oslofjorden contrasts the values observed in Lindåspollene and Boknafjorden (Table 2). The chlorophyll maximum and the nutricline depth were undoubtedly shallowest in Oslofjorden with a depth of 8 and 4.5 m, respectively. Boknafjorden had a chlorophyll maximum of around 17 m and a nutricline depth of 19 m. Lindåspollene had the deepest chlorophyll maximum located at 25 m, and a nutricline depth of 17 m.

Simulated vertical structures

The salinity proxy, using the observed average salinity between the surface and the depth of the chlorophyll maximum, was used to calculate the background attenuation (K_{bg}) from Eq. (9) (See section 2.3.1). Further, the turbulent diffusivities at each location were approximated from the observed stratification, computed from the variables salinity and temperature, using Eqs. (10), (11) and (12) (section 2.3.1). The nitrate concentration in last depth cell (N_B), i.e. the depth at 50 m, was chosen according to the observed nitrate concentration at the different locations, i.e. 15, 15 and 30 mmol N m^{-3} for Lindåspollene, Boknafjorden and Oslofjorden, respectively.

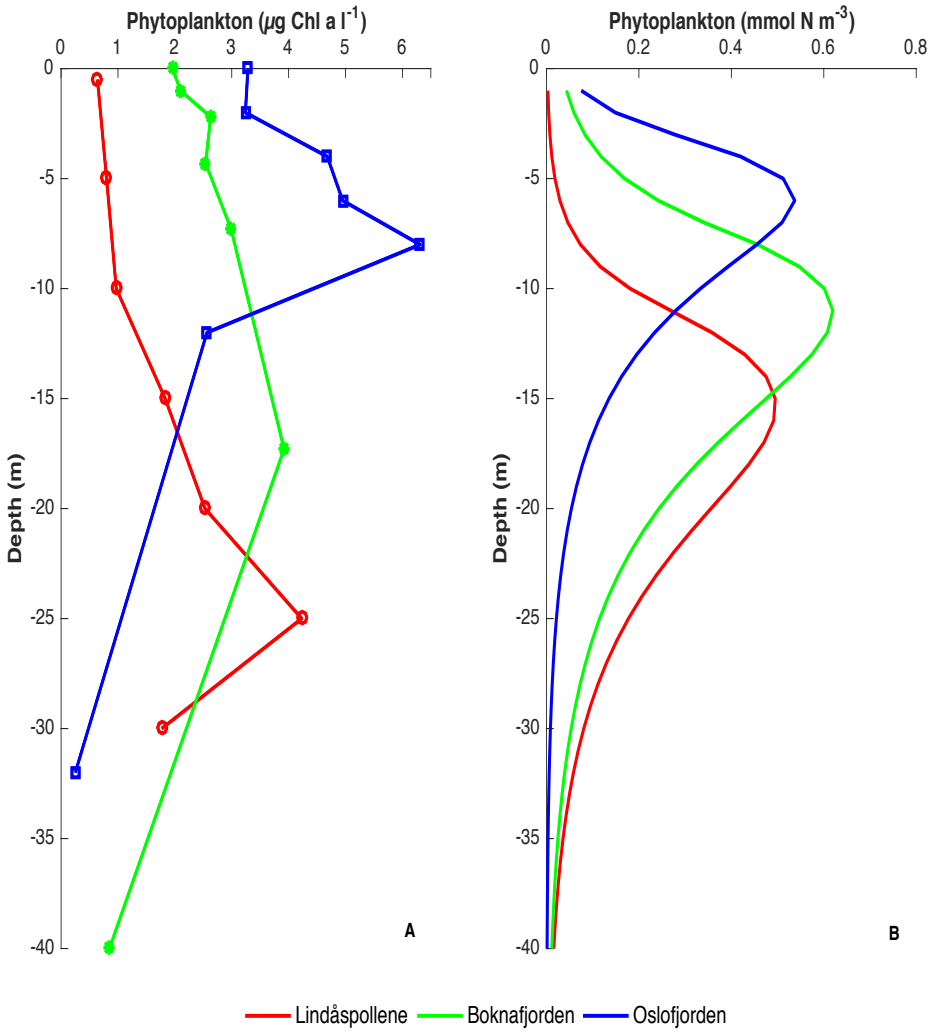

Figure 4. Observed vertical distribution of phytoplankton (A) during summer in Lindåspollene (Erga and Skjoldal, 1990), Boknafjorden (Erga, 1989a; Erga, 1989b) and Oslofjorden (Paasche and Erga, 1988), and the simulated vertical distribution of phytoplankton (B) for the same locations. Note the different units of observed and simulated phytoplankton concentration, i.e. µg Chl a l^{-1} and mmol N m^{-3}, respectively.

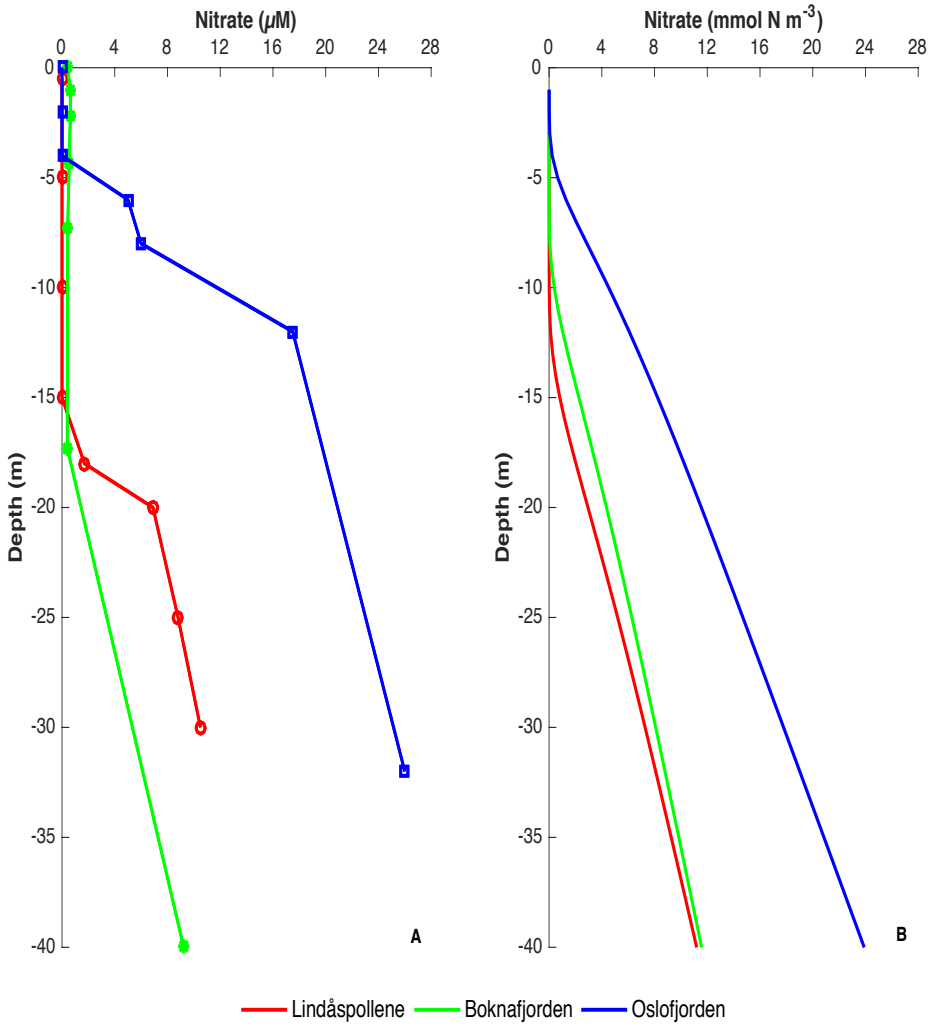

Figure 5. Observed vertical distribution of nitrate (A) during summer in Lindåspollene (Erga and Skjoldal, 1990), Boknafjorden(Erga, 1989a; Erga, 1989b) and Oslofjorden (Paasche and Erga, 1988), and the simulated vertical distribution of nitrate (B) for the same locations.

Observations vs. simulations

Although the simulations of the nutrient concentration do not show the exact same as the observed values (Fig. 5), which is not expected from an idealized model that has not been fitted to the observation, it shows similar trends in terms of the nutricline (Fig. 5) and nutricline depth of the three fjords (Table 2). The simulated chlorophyll maximum depth showed similar consistencies with the observations in the three fjords (Fig. 4 and Table 2). The background attenuation applied in the simulations was highest for Oslofjorden since it had the lowest salinity out of all three locations (Table 2). In terms of turbulent diffusivity (κ), Boknafjorden had the highest κ in the

simulation, whereas the lowest κ was approximated for Oslofjorden (Table 2) due to stronger density stratification.

Table 2. Parameter values (in bold) of the background attenuation ($\mathbf{K_{bg}}$), vertical turbulent diffusivity ($\boldsymbol{\kappa}$) and nutrient concentration at Z_{50} ($\mathbf{N_B}$), i.e. the nitrate concentration in last depth cell (50 m), used in the simulations. The choice of the different values is explained in section 2.3.1. The resulting simulated values of the euphotic depth (Z_E), Secchi depth (Z_S), and nutricline depth (Z_N) (see section 2.3.2), and the depth of the Chlorophyll a maximum (Chl_{max}) for Lindåspollene, Boknafjorden and Oslofjorden are also included.

Variables	Units		Lindåspollene	Boknafjorden	Oslofjorden
K_{bg}	**m^{-1}**		**0.22**	**0.28**	**0.61**
κ	**m^2s^{-1}**		**$2.54x10^{-5}$**	**$3.5x10^{-5}$**	**$1.22x10^{-5}$**
N_B	**mmol N m^{-3}**		**15**	**15**	**30**
Z_E	m	Simulated	17.6	13.5	7.2
		Observed	20	17.3	—
Chl_{max}	m	Simulated	15	11	6
		Observed	25	17.3	8
Z_N	m	Simulated	16	12	6
		Observed	17	19	4.5
Z_S	m		6.8	5.1	3.0

3.2 Temporal trends in summer temperature and salinity at two coastal stations

Data from IMRs fixed hydrographic stations at Lista and Sognesjøen made it possible to collect information about changes in summer temperature and salinity (i.e. from June to August), thus also density as it is controlled by these two properties. The salinity changes served as an indicator of changes in the K_{bg} (see section 2.3.1), whilst temperature and salinity changes were used to provide information about variations in stratification and/or stability, which again was used to approximate changes in the turbulent diffusivity (κ) (see section 2.3.1).

Based on data from Lista and Sognesjøen, temperature, salinity and density were plotted at depths of 10 and 50 m against time (Figs. 6 and 7). Further, a simple linear regression was calculated to assess how temperature, salinity and density have changed over the past decades.

Lista

The temporal changes in temperature, salinity and density at station Lista are shown in Fig. 6. The slope of the regression line for temperature at Lista is positive, suggesting that the temperature has increased from 1942 to 2012. Temperature both at 10 and 50 m at Lista showed significant *p*-values ($p < .01$) (Fig. 6). For salinity the opposite trend was observed, having a negative slope of the line, suggesting a decrease in salinity over the same period. However, the regression lines for salinity only showed a significant *p*-value at 10 meter ($p = .025$) (Fig. 6). The slope of the regression line for density is also negative, suggesting a decrease in density from 1942 to 2012. The regression lines for density showed significant *p*-values both at 10 and 50 meter ($p < .01$ and $p = .018$, respectively) (Fig. 6).

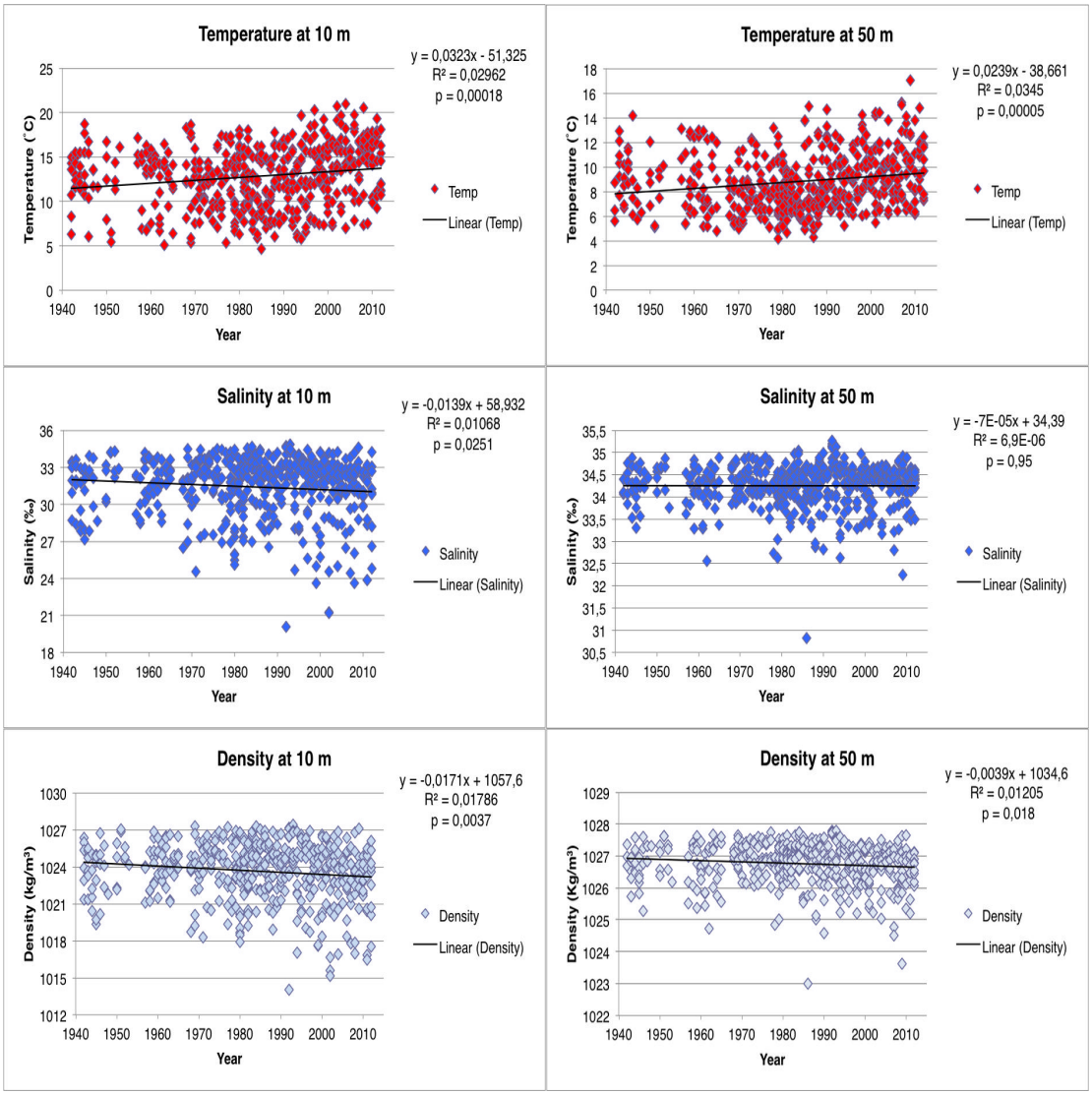

Figure 6. Linear regression analysis of temperature (red), salinity (blue) and density (grey) at station Lista for 10 m (left column) and 50 m (right column) in the summer months June–August in the period 1942 –2012.

Sognesjøen

The temporal changes in temperature, salinity and density at station Sognesjøen are shown in Fig. 7. The slope of the regression line for temperature at Sognesjøen is also positive, suggesting that the temperature here has increased from 1935 to 2012 at a depth of 10 m ($p < .01$) and of 50 m ($p < .01$). The slope of the regression line for salinity is negative, suggesting that the salinity has decreased from 1935 to 2012. However, there were no significant *p*-values for the regression lines for salinity at 10 and 50 m ($p = 0.38$ and $p = 0.93$, respectively) (Fig. 7). Similarly, the slope of the

regression line for density is also negative and the regression line did not show significant *p*-values at either 10 or 50 m ($p = .069$ and $p = .086$, respectively) (Fig. 7).

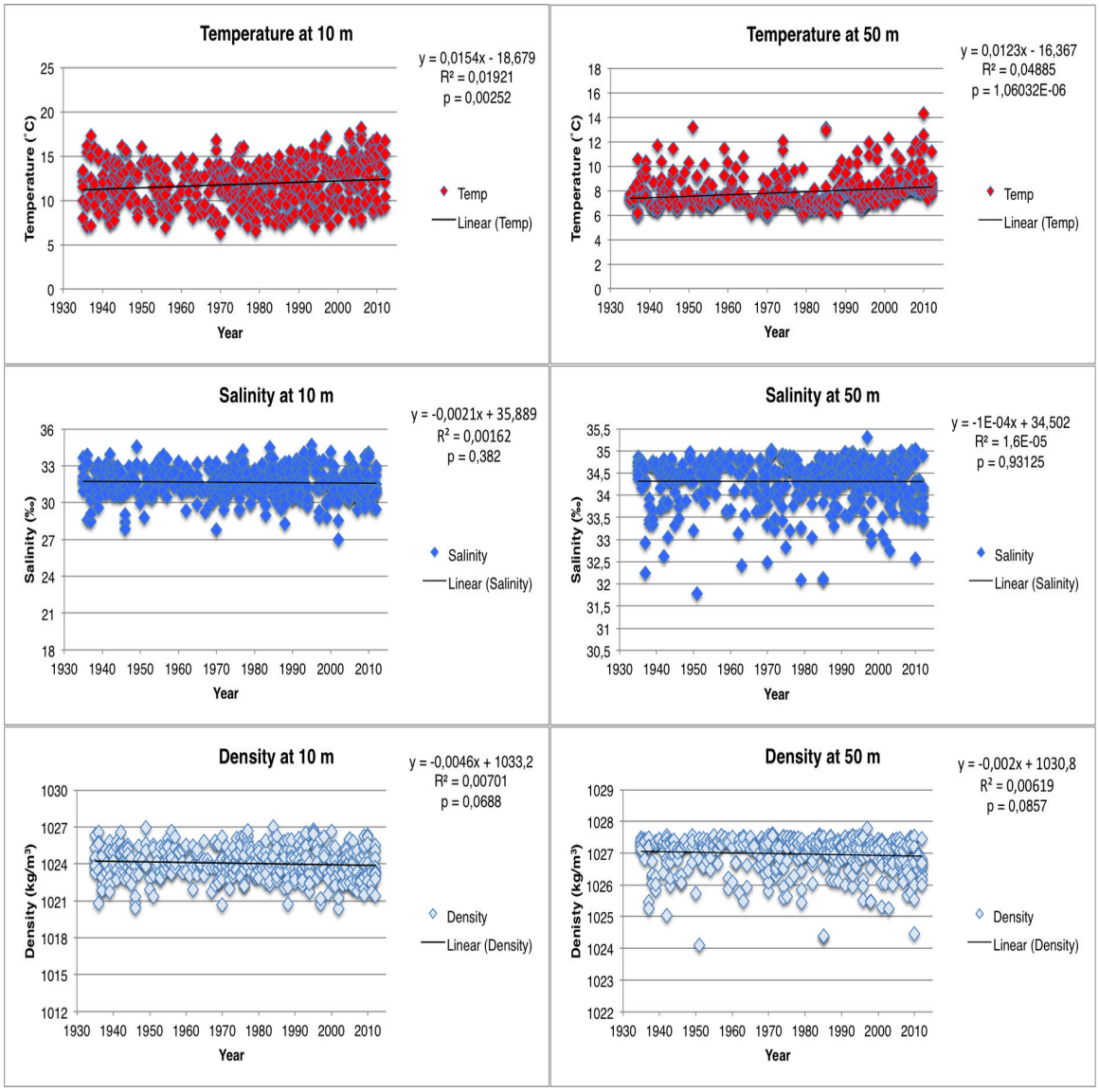

Figure 7. Linear regression analysis of temperature (red), salinity (blue) and density (grey) at station Sognesjøen for 10 m (left column) and 50 m (right column) in the summer months June–August in the period 1935–2012.

3.3 Past and future simulated scenarios of NCW euphotic properties

The vertical distribution of phytoplankton and nitrate concentration and the other euphotic zone properties (see section 2.3.2) were simulated for a past, present and future scenario at Lista and in Sognesjøen.

This section will focus on potential changes in the background attenuation (K_{bg}), (1) how it may have changed in the past, (2) may change in the future, and (3) in what way changes in this parameter may affect the euphotic zone properties. Here, I have assumed the turbulent diffusivity (κ) to be constant.

Firstly, K_{bg} was determined for a present scenario using the salinity proxy from Eq. (9) (section 2.3.1). From the Secchi depth observations, a K_{bg} was approximated for the past scenario from Eq. (16) (section 2.4.2). From a projected increase in the concentration of organic carbon (OC), a K_{bg} was approximated for both a future 1 and future 2 scenario from Eq. (17) and (18), respectively (section 2.4.3).

Lista

For simulations of the vertical distribution at Lista (Fig. 8), a mean salinity of 31.2 ‰ was used in all scenarios, which was the mean salinity down to 30 m in year 2010 (present). This corresponds to a K_{bg} of 0.172, 0.191, 0.234 and 0.298 m^{-1} for a past (1942), present (2010), future 1 (1950) and future 2 (2100) scenario, respectively. A turbulent diffusivity of κ = 5,18 $\times 10^{-5}$ m^2 s^{-1}, based on the differences in density between 10 and 50 m at Lista in 2010 (present) (Fig. 6), was used for all the simulated scenarios. The values of the input parameters (K_{bg}, κ, and N_B), along with the different simulated euphotic zone properties are listed in Table 3.

A simulation of a past scenario (Fig. 8A) using a K_{bg} = 0.172 m^{-1}, indicated a euphotic depth (Z_E) at 18.3 m, a Secchi depth (Z_S) around 7.5 m, and a nutricline depth (Z_N) at 16 m. For simulation of the present scenario (Fig. 8B), using a K_{bg} = 0.191 m^{-1}, a euphotic depth (Z_E) of approximately 17 m were obtained, together with a Secchi depth (Z_S) of around 6.9 m and a nutricline depth (Z_N) of 15 m. Note that even a small

increase in K_{bg}, from 0.172 to 0.192 m^{-1}, a decrease in the euphotic depth was observed, along with a decrease in both Secchi depth and nutricline depth (Table 3). The highest background attenuation (K_{bg} = 0.298 m^{-1}) was approximated for the future 2 scenario. For this scenario (Fig. 8D), the euphotic depth (Z_E) was located at approximately 12 m, suggesting a decrease of around 5 m from a euphotic depth of about 17 m in the present scenario. Moreover, a Secchi depth shoaling of about 2.5 m, and a 5 m decrease in the nutricline depth from the present to the future scenario was also observed.

It was also observed a decrease in the surface integrated biomass of phytoplankton (Bi), and the surface integrated primary production (Pi) over the simulated period (1942–2100) (Table 3). The average nutrient concentration in the upper 20 m (SumN) however, increased from 0.55- to 1.6 mmol N m^{-2} over the same time period (Table 3).

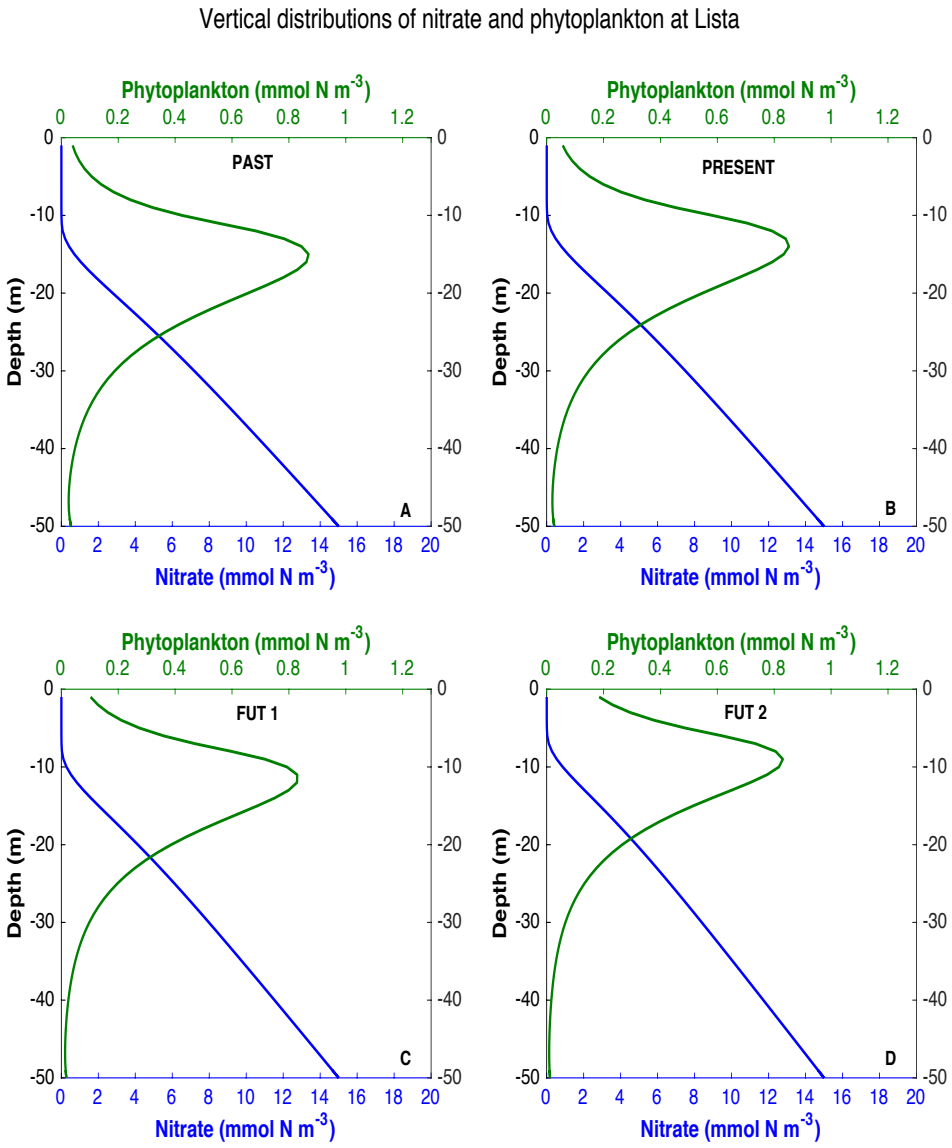

Figure 8. Simulated vertical distributions of phytoplankton and nitrate concentration for a summer situation at Lista for a past (A), present (B), future 1 (C) and future 2 (D) scenario using a constant turbulent diffusivity ($\kappa = 5{,}18 \times 10^{-5}\ m^2\ s^{-1}$). See Table 3 for values of the input parameters (K_{bg}, κ, and N_B) and the different simulated euphotic zone properties.

Table 3. Values of input parameters (***K_{bg}*, *κ*, and *N_B*)** in bold and different simulated euphotic zone properties for a past (1942), present (2010), future 1 (2050) and future 2 (2100) scenario representing a summer situation (June–August) at Lista.

Variables	Units	Past (1942)	Present (2010)	Future 1 (2050)	Future 2 (2100)
K_{bg}	m^{-1}	0.172	0.191	0.234	0.298
κ	m^2s^{-1}	5.18×10^{-5}	5.18×10^{-5}	5.18×10^{-5}	5.18×10^{-5}
N_B	mmol N m^{-3}	15	15	15	15
Z_E	m	18.30	16.95	14.34	11.87
Z_S	m	7.56	6.87	5.61	4.49
Z_N	m	16	15	12	10
sumN	mmol N m^{-2}	0.55	0.75	1.16	1.63
Bi	mmol N m^{-2}	14.12	13.63	12.85	12.16
Pi	mmol N $m^{-2}h^{-1}$	0.14	0.136	0.129	0.122

Sognesjøen

For simulations of the vertical distribution in Sognesjøen (Fig. 9), a mean salinity of 32.1 ‰ was used for all scenarios, which was the mean salinity down to 30 m in year 2010 (present). This corresponds to a K_{bg} of 0.143, 0.154, 0.185 and 0.237 m^{-1} for the past (1935), present (2010), future 1 (2050) and future 2 (2100) scenario, respectively. A turbulent diffusivity of $\kappa = 6.48 \times 10^{-5}$ m^2 s^{-1}, based on differences in density at 10 and 50 m in Sognesjøen in 2010 (present) (Fig. 7), was used for all the simulated scenarios. Table 4 display values of the input parameters (K_{bg}, κ, and N_B), along with the different simulated euphotic zone properties.

Although the euphotic, Secchi and nutricline depth was located slightly deeper in the water column in Sognesjøen, the simulated vertical distributions of nitrate and phytoplankton in the different scenarios (Fig. 9 and Table 4) showed similar trends as for the simulations at Lista (See Fig. 8 and Table 3).

Simulation of a past scenario (Fig. 9A), with a $K_{bg} = 0.143$ m^{-1}, provided a euphotic depth (Z_E) at approximately 19.5 m, a Secchi depth (Z_S) around 8 m, and a nutricline depth (Z_N) at 17 m. For a simulated present scenario (Fig. 9B), using a $K_{bg} = 0.154$ m^{-1}, a euphotic depth (Z_E) around 18.5 m was obtained, together with a Secchi depth located approximately at 7.7 m and a nutricline depth (Z_N) of 16 m. The highest background attenuation ($K_{bg} = 0.237$ m^{-1}) was approximated for the future 2 scenario

(2100). For a simulated future 2 scenario (Fig. 9D), the euphotic depth was located at approximately 13.5 m, suggesting a decrease of around 5 m in euphotic depth from the present scenario. Moreover, a Secchi depth shoaling of about 2.5 m, and a 4 m decrease in the nutricline depth from the present to a future 2 scenario were also observed (Table 4).

Similar to Lista, it was also observed a decrease in the surface integrated biomass of phytoplankton (Bi), including the surface integrated primary production (Pi) over the simulated period (1935–2100) in Sognesjøen (Table 4). The average nutrient concentration in the upper 20 m (SumN) also increased from the past to a future 2 scenario in Sognesjøen (Table 4).

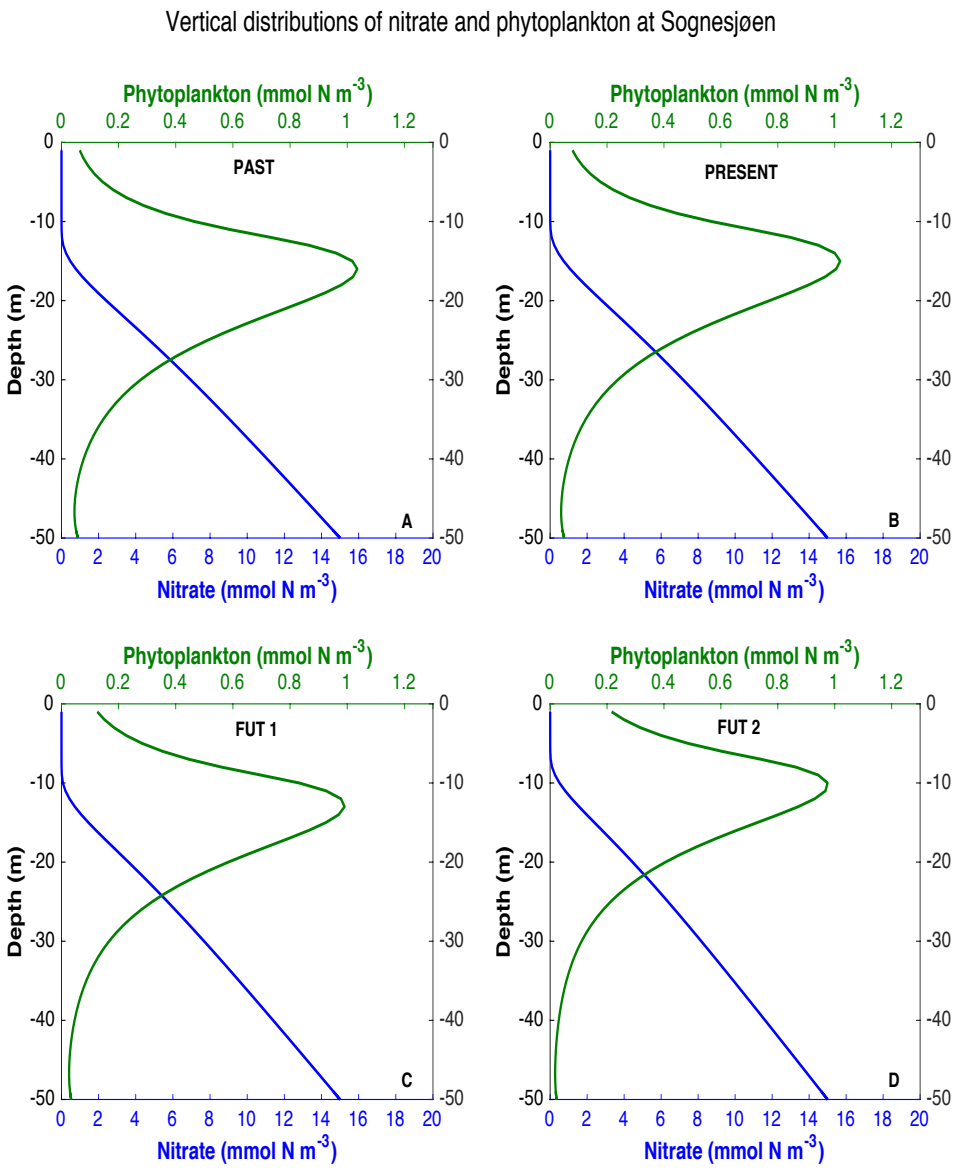

Figure 9. Simulated vertical distributions of phytoplankton and nitrate concentration for a summer situation in Sognesjøen for a past (A), present (B), future 1 (C) and future 2 (D) scenario using a constant turbulent diffusivity (κ = 6,48 $\times 10^{-5}$ m^2 s^{-1}). See Table 4 for values of the input parameters (K_{bg}, κ, and N_B) and the different simulated euphotic zone properties.

Table 4. Values of input parameters (***K_{bg}*, *κ*, and *N_B*)** in bold and different simulated euphotic zone properties for a past (1935), present (2010), future 1 (2050) and future 2 (2100) scenario representing a summer situation (June–August) in Sognesjøen.

Variables	Units	Past (1935)	Present (2010)	Future 1 (2050)	Future 2 (2100)
$\mathbf{K_{bg}}$	m^{-1}	0.143	0.154	0.185	0.237
$\boldsymbol{\kappa}$	m^2s^{-1}	6.48×10^{-5}	6.48×10^{-5}	6.48×10^{-5}	6.48×10^{-5}
$\mathbf{N_B}$	mmol N m^{-3}	15	15	15	15
Z_E	m	19.45	18.44	16.08	13.39
Z_S	m	8.18	7.72	6.44	5.08
Z_N	m	17	16	14	12
sumN	mmol N m^{-2}	0.44	0.56	0.89	1.35
Bi	mmol N m^{-2}	18.04	17.59	16.63	15.63
Pi	mmol N $m^{-2}h^{-1}$	0.18	0.176	0.17	0.16

3.4 Simulated effects of changes in density stratification and background attenuation

In the previous simulations, the background attenuation (K_{bg}) was the only parameter that varied between the different scenarios. In this section, variations in turbulent diffusivity (κ) was also applied for the past, present and future scenario. Here, I did not include the future 1 scenario, i.e. year 2050.

For the past and present scenario, the buoyancy frequency (N) was calculated according to Eq. (11) from the differences observed in density at 10 and 50 m from station Lista and Sognesjøen. Density differences were extrapolated into the future. The buoyancy frequency for the future was calculated from the extrapolated density differences according to Eq. (11). Further, the turbulent diffusivities for the different scenarios were approximated according to Eq. (10) and Eq. (12) (See section 2.3.1).

Lista

From density differences between 10 and 50 m (Table 5), the buoyancy frequency for the past (1942), present (2010) and future (2100) scenario was calculated (Eq. 11). Further, the turbulent diffusivities were approximated (Eq.10), corresponding to a κ-value of 6.96×10^{-5}, 5.18×10^{-5} and 3.87×10^{-5} $m^2\ s^{-1}$ for the past, present and future scenario, respectively. The input parameters used, along with the simulated euphotic zone properties are listed in Table 6.

Table 5. Trendline equations (see Fig. 6) and density differences between 10 and 50 m for a summer situation (June–August) at Lista in the past (1942) and the present (2010), including extrapolated density differences for the future (2100). The calculated squared buoyancy frequencies (N^2) for the different scenarios are also included (See section 2.3.1).

	a	**b**	**Past (1942)**	**Present (2010)**	**Future (2100)**
10 m	-0.0171	1057.6	1024.39	1023.23	1021.69
50m	-0.0039	1034.6	1027.03	1026.76	1026.41
$\boldsymbol{dr}$			2.63	3.53	4.72
$\boldsymbol{dr/dz}$			0.065	0.088	0.118
$\boldsymbol{r\_mean}$			1025.71	1024.99	1024.05
$\boldsymbol{N^2}$			6.29E-04	8,44E-04	1.13E-03

Simulations of vertical distributions with variation in κ and K_{bg} for the past, present and future scenarios at Lista are shown in Fig. 10. For a simulated past scenario (Fig. 10A), the K_{bg} was approximated from Eq. (16) from a salinity of 32 ‰, which was the mean salinity down to 25 m in 1942 at Lista and corresponding to a $K_{bg} = 0.146\ m^{-1}$. Hence, simulation of vertical distribution for the past scenario, with $K_{bg} = 0.146\ m^{-1}$ and $\kappa = 6.96\times10^{-5}\ m^2 s^{-1}$, provided a euphotic depth (Z_E) of 18.7 m, a Secchi depth (Z_S) of 7.9 m and a nutricline depth (Z_N) of 16 m (Table 6). For comparison, the euphotic depth was located at 18.3 m, the Secchi depth at 7.5 m and the nutricline depth at 16 m for simulation of the past scenario using a constant κ (Table 3).

For the future scenario the K_{bg} was kept unchanged, corresponding to a $K_{bg} = 0.298\ m^{-1}$ (i.e. similar to the previous simulated future scenario at Lista, Table 3). This was done to observe the effect of turbulent diffusivity. Also, density extrapolation (Table 5) gave rise to a turbulent diffusivity of $\kappa = 3{,}87\times10^{-5}\ m^2 s^{-1}$. From this, simulations of a future scenario (Fig. 10C) resulted in a euphotic depth (Z_E) of 12.5 m, a Secchi depth (Z_S) around 4.9 m and a nutricline depth (Z_N) of 11 m. For comparison, the euphotic depth was located at 11.9 m, the Secchi depth at 4.5 m and the nutricline depth at 10 m for simulations using a constant κ for a future scenario (See Table 3).

The approximated turbulent diffusivities from the observed density differences, i.e. "true" κ, decreased from the past to the future scenario (from $\kappa = 6.96\times10^{-5}\ m^2 s^{-1}$ to $\kappa = 3.87\times10^{-5}\ m^2 s^{-1}$) (Table 6).

Simulations of the past, present and a future scenario with variation in turbulent diffusivity (Fig. 10 and Table 6) show minor differences in the euphotic depth, Secchi depth and nutricline depth from the past to a future scenario by comparing those with simulations using a constant turbulent diffusivity (Fig 8 and Table 3). The surface integrated biomass of phytoplankton (Bi) was however slightly higher using a "true" and somewhat higher turbulent diffusivity ($\kappa = 6.96\times10^{-5}$ m ^{2}s^{-1}) for the past scenario, i.e. 18.93 mmol N m^{-2} (Fig. 10A), compared to the simulated past scenario using a constant κ ($\kappa = 5.18\times10^{-5}$ m ^{2}s^{-1}), i.e. Bi = 14.12 mmol N m^{-2} (Fig. 8A). For the future scenario, the surface integrated biomass of phytoplankton (Bi) was somewhat lower using a "true" turbulent diffusivity ($\kappa = 3.87\times10^{-5}$ m ^{2} s^{-1}), i.e. 9.29 mmol N m^{-2} (Fig. 10C), compared to the simulation using a constant turbulent diffusivity ($\kappa = 5.18\times10^{-5}$ m ^{2}s^{-1}), i.e. Bi = 12.16 mmol N m^{-2} (Fig. 8D). A similar decreasing trend from past to future could also be observed for the surface integrated primary production (Pi).

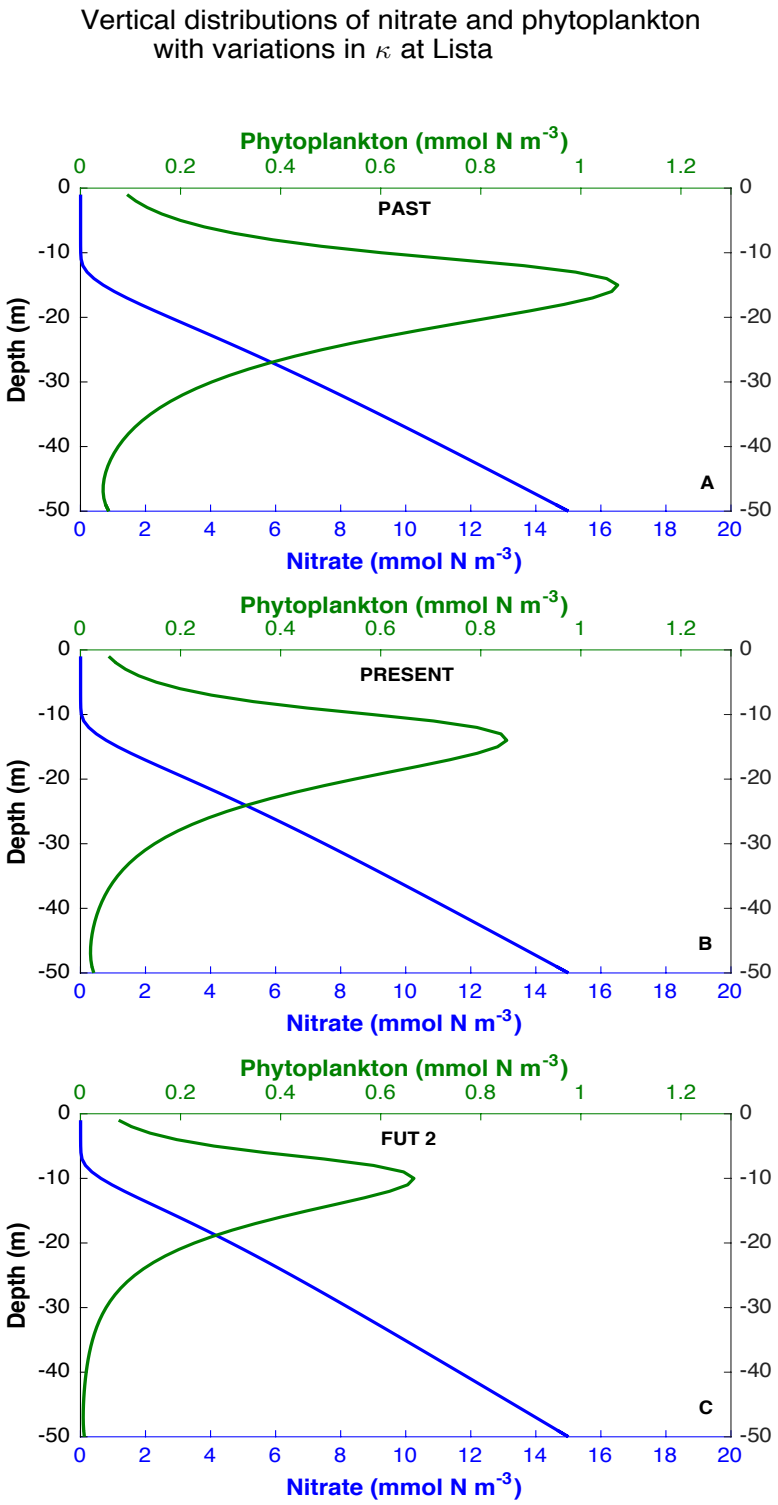

Figure 10. Simulated vertical distributions of phytoplankton and nitrate concentration with variations in turbulent diffusivity (κ), i.e. "true κ", for a summer situation at Lista for a past (A), present (B), and future (C) scenario. See Table 6 for values of the input parameters (K_{bg}, κ, and N_B), along with the different simulated euphotic zone properties.

Table 6. Simulated effects of changes in density stratification. Values of input parameters ($\mathbf{K_{bg}}$, **κ,** and $\mathbf{N_B}$) in bold and the different simulated euphotic zone properties for a past (1942), present (2010) and future (2100) scenario representing a summer situation (June–August) at Lista.

Variables	Units	Past (1942)	Present (2010)	Future (2100)
$\mathbf{K_{bg}}$	m^{-1}	0.146	0.191	0.298
$\boldsymbol{\kappa}$	m^2s^{-1}	6.96×10^{-5}	5.18×10^{-5}	3.87×10^{-5}
$\mathbf{N_B}$	mmol N m^{-3}	15	15	15
Z_E	m	18.67	16.95	12.54
Z_S	m	7.87	6.87	4.85
Z_N	m	16	15	11
sumN	mmol N m^{-2}	0.54	0.75	1.46
Bi	mmol N m^{-2}	18.93	13.63	9.29
Pi	mmol N $m^{-2}h^{-1}$	0.189	0.136	0.093

Sognesjøen

From density differences between 10 and 50 m (Table 7), the buoyancy frequency for the past (1935), present (2010) and a future (2100) scenario was calculated (Eq. 11). Further, the turbulent diffusivities were approximated (Eq.10), corresponding to a κ-value of 6.96×10^{-5}, 6.48×10^{-5} and 5.98×10^{-5} $m^2\ s^{-1}$ for the past, present and future scenario, respectively. The input parameters used, along with the simulated euphotic properties are listed in Table 8.

Table 7. Trendline equations (see Fig. 7) and density differences between 10 and 50 m for a summer situation (June–August) at Sognesjøen in the past (1935) and present (2010), including extrapolated density differences for the future (2100). The calculated squared buoyancy frequencies (N^2) for the different scenarios are also included (See section 2.3.1).

	a	**b**	**Past (1935)**	**Present(2010)**	**Future(2100)**
10 m	-0,0046	1033,2	1024,30	1023,95	1023,54
50m	-0,002	1030,8	1026,93	1026,78	1026,6
$\boldsymbol{dr}$			2,63	2,83	3,06
$\boldsymbol{dr/dz}$			0,066	0,071	0,077
$\boldsymbol{r\_mean}$			1025,61	1025,37	1025,07
$\boldsymbol{N^2}$			6,28E-04	6,75E-04	7,31E-04

Simulations of the vertical distribution with variation in κ in Sognesjøen for the past, present and future scenarios are shown in Fig. 11. For a simulated past scenario (Fig. 11A), the K_{bg} was approximated from Eq. (16) for a salinity of 30.1 ‰, which was the mean salinity down to 25 m in 1935 in Sognesjøen and corresponded to a K_{bg} = 0.207 m^{-1}.

A simulated past scenario (Fig. 11A), using K_{bg} = 0.207 m^{-1} and $\kappa = 6.96\times10^{-5}$, provided a euphotic depth (Z_E) of 14.5 m, a Secchi depth (Z_S) of 5.7 m and a nutricline depth (Z_N) of 12 m. For comparison, the euphotic depth was located at 19.5 m, the Secchi depth at 8.2 m and the nutricline depth at 17 for the simulation of a past scenario using a constant κ (Table 4).

For the future scenario the K_{bg} was kept unchanged, corresponding to a K_{bg} = 0.237 m^{-1} (i.e. similar to the previous simulated future scenario at Sognesjøen, Table 4). This was done to observe the effect of turbulent diffusivity. Also, density extrapolation (Table 7) gave rise to a turbulent diffusivity of $\kappa = 5{,}98 \times10^{-5}$ $m^2\,s^{-1}$. From this, simulations of a future scenario (Fig. 11C) resulted in a euphotic depth (Z_E) of 13.7 m, a Secchi depth (Z_S) around 5 m and a nutricline depth (Z_N) of 12 m. For comparison, the euphotic depth was located at 13.5 m, the Secchi depth at 5 m and the nutricline depth at 12 m for simulations using a constant κ for a future scenario (Table 4).

Note, the background attenuation was much higher in the in the past scenario using a varied κ (Table 8) than for the simulated past scenario using constant κ (Table 4). The higher background attenuation is due to fresher water in Sognesjøen in the past compared to the present (salinity as a proxy for K_{bg}, Eq. 16). Hence, the large differences observed in the euphotic depth, Secchi depth and nutricline depth by comparing the two past scenarios (Tables 4 and 8), was most likely due to the variation in K_{bg} and not the variation in κ. Comparing the simulated future scenarios (having the same K_{bg}), one using a constant κ the other a varied κ, reinforced this claim as they show similar trends and very small differences in euphotic depth, Secchi depth and nutricline depth (Tables 4 and 8).

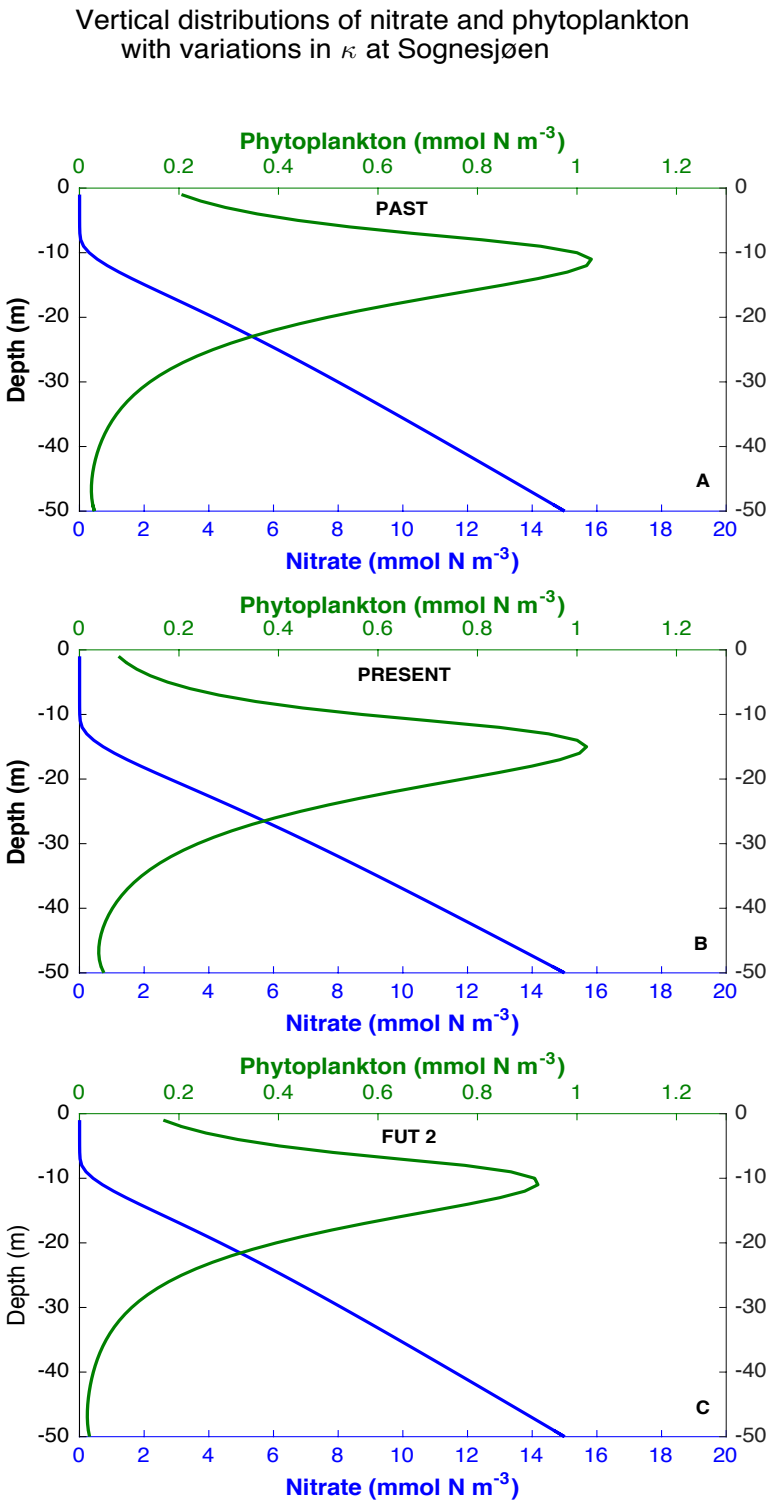

Figure 11. Simulated vertical distributions of phytoplankton and nitrate concentration with variations in turbulent diffusivity (κ), i.e. with a "true" κ, for a summer situation in Sognesjøen for a past (A), present (B), and future (C) scenario. See Table 8 for values of the input parameters (K_{bg}, κ, and N_B) and the different simulated euphotic zone properties.

Table 8.Simulated effects of changes in density stratification.Values of input parameters (**K_{bg}, κ, and N_B)** in bold, along with different simulated euphotic zone properties for a past (1935), present (2010) and future (2100) scenario representing a summer situation (June–August) at Sognesjøen.

Variables	Units	Past (1935)	Present (2010)	Future (2100)
K_{bg}	m^{-1}	0.207	0.154	0.237
κ	m^2s^{-1}	6.96×10^{-5}	6.48×10^{-5}	5.98×10^{-5}
N_B	mmol N m^{-3}	15	15	15
Z_E	m	14.52	18.43	13.73
Z_S	m	5.69	7.72	5.25
Z_N	m	12	16	12
sumN	mmol N m^{-2}	1.16	0.55	1.29
Bi	mmol N m^{-2}	17.16	17.59	14.56
Pi	mmol N $m^{-2}h^{-1}$	0.172	0.176	0.146

3.5 Implication of variation in K_{bg} of NCW

In this section the predicted variation in euphotic depth, Secchi depth, and nutricline depth as a function of salinity was simulated for the past, present and future. The salinity range was set to span from 24 to 35. The resulting simulated values of the euphotic depth (Z_E), Secchi depth (Z_S), and nutricline depth (Z_N) are explained in section 2.3.2 (the input and output values can be viewed in Appendix B, Table 1–3).

The input parameters κ and N_B was set constant throughout the simulated scenarios i.e. $\kappa = 5.18\times10^{-5}$ and $N_B = 15$ (same as for station Lista). For a past scenario, the background attenuation (K_{bg}) was derived from salinity according to Eq. (16) (section 2.4.2). For the present scenario, K_{bg} was derived from salinity according to Eq, (9) (section 2.3.1) and for the future scenario, i.e. future 2, K_{bg} was derived from salinity according to Eq. (18) (section 2.4.3).

From Fig. 12 (A) it can be observed that the euphotic depth (Z_E) is much shallower in NCW_{24} than for the euphotic depth in NAW_{35}. In the past scenario the euphotic zone was approximately 29 m shallower in the NCW_{24} than in NAW_{35} (9 and 38 m for NCW_{24} and NAW_{35}, respectively). In the present scenario, the euphotic depth was approximately 33 m shallower in the NCW_{24} than in NAW_{35} (8 and 41 m, respectively) and in the future scenario the euphotic depth was 35 m shallower in the

NCW_{24} than in NAW_{35} (5 and 40 m, respectively). The euphotic depth has moved upward, i.e. decreased in meters, from the past to a simulated future. This was particularly true for the salinity variation from 24 to 33. For salinities in the upper range (i.e. between 34 and 35), the euphotic depths in the different scenarios had a tendency to overlap, which might be due to inaccuracies in the computations when the background attenuation approaches 0.03 m^{-1} (i.e. that assumed for NAW, see section 2.3.1).

The Secchi depth has also moved upwards, i.e. decreased in meters from past till future, for salinities between 24 and 34 (Fig. 12B). For the past, the Secchi depth corresponded to 4 and 24 m for NCW_{24} and NAW_{35}, respectively. In the present, it corresponded to 3 and 30 m for NCW_{24} and NAW_{35}, respectively. And for the future scenario, the Secchi depth corresponded to 2 and 27 m for NCW_{24} and NAW_{35}, respectively. As for the euphotic depth, the Secchi depths in the different scenarios showed a tendency to overlap at salinity variations in the upper range.

The nutricline depths showed similar trends as for the euphotic depths and Secchi depths (Fig. 12C). For the past, the nutricline depth corresponded to 8 and 34 m for NCW_{34} and NAW_{35}, respectively. In the present scenario, the nutricline depth corresponded to 7 and 38 for NCW_{24} and NAW_{35}, respectively. And for the future scenario, the nutricline depth corresponded to 5 and 36 m for NCW_{24} and NAW_{35}, respectively.

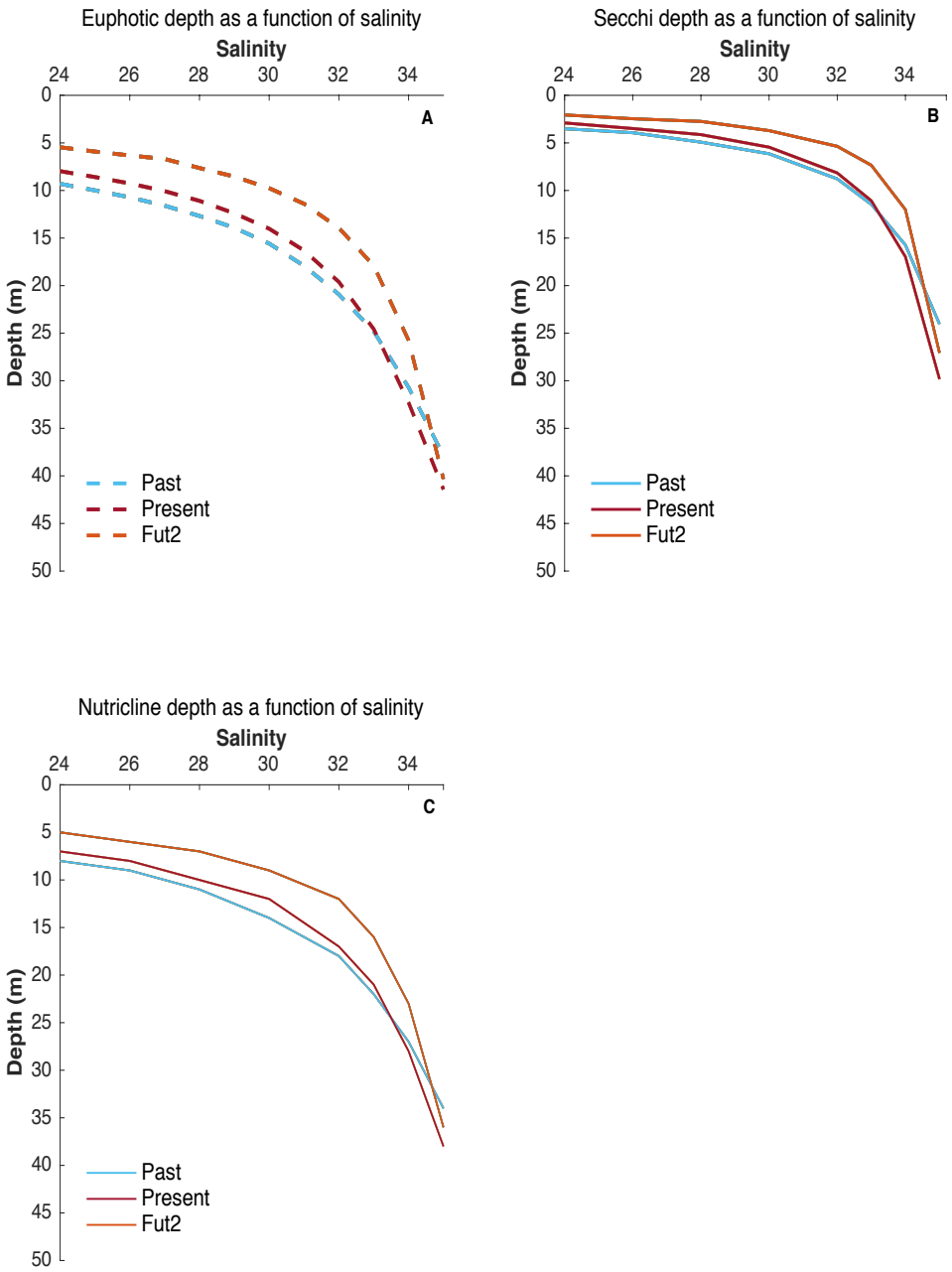

Figure 12. Simulated variations in euphotic depth (A), Secchi depth (B), and nutricline depth (C) as a function of salinity in a gradient from NCW_{24} to NAW_{35} (i.e. salinity range from 24 to 35) for a past, present and future scenario (see Appendix B, Table 1–3).

4 DISCUSSION

The idealized simulation model of Huisman et al. (2006) was used to simulate vertical distributions of nitrate and phytoplankton and associated euphotic zone properties. The simulations were to represent the NCW ecosystems along southwestern Norway during an idealized summer situation. The objective was to observe how these NCW properties would respond to changes in light absorption associated with background attenuation (K_{bg}), i.e. CDOM of terrestrial origin, for the past, present and the future.

A summer situation was chosen, as it resembles a steady state situation, i.e. the amount of input equals the amount of output, which the simulation model of Husiman et al. (2006) was "designed" for. In fjords and polls, this season is characterized by strong density stratification due to high incoming solar radiation, and as a result of maximum freshwater runoff (Sætre and Ljøen, 1972; Erga, 1989a; Erga et al., 2012), and calm wind condition along the coast (Aure et al, 2007).

A modification of the simulation model of Huisman et al. (2006) was done. The modification was applied to the self-shading of phytoplankton, because coastal waters tend to be more eutrophic than the oligotrophic subtropical water studied by Huisman et al. (2006). While Huisman et al. (2006) kept the background attenuation (K_{bg}) constant and low, I have adjusted the K_{bg}, similar to Urtizberea et al. (2013). However, Urtizberea et al. (2013) varied K_{bg} over a limited range (i.e. 0.03–0.2 m^{-1}) and was a purely theoretical study not aimed to represent a particular location. In my study, different data sources were used to study the K_{bg} variations reflecting the NCW in the past, present and for the future.

Simulations versus observations in the three fjords

The observed vertical distributions of nitrate and phytoplankton concentration in the three fjords, i.e. Lindåspollene, Boknafjorden and Oslofjorden, were compared to simulated vertical structures (section 3.1). The simulation results were consistent with the observations in the sense that the shallowest vertical distribution of nutrient and phytoplankton was found in Oslofjorden, while Lindåspollene had the deepest

chlorophyll maximum in both the observed and simulated vertical structures. The vertical distribution of nitrate and phytoplankton in Boknafjorden was located somewhere in between the two other locations (Fig. 4 and 5, and Table 2). In terms of turbulent diffusivity (κ), the highest value was approximated for Boknafjorden, while Oslofjorden had the lowest. However, the observed phytoplankton distribution in Boknafjorden was not very pronounced (Fig. 4A) whereas the simulated distribution of phytoplankton showed a very distinct peak (Fig. 4B). This could mean that the turbulent diffusivity in reality is even higher than the approximated value for Boknafjorden. The highest background attenuation (K_{bg}) was approximated for the fjord that had the lowest salinity, i.e. Oslofjorden and consequently the highest background attenuation. This is a direct result of the salinity proxy that has been used and the data that have formed the basis for this proxy in Aksnes, 2015. Such negative correlation between salinity and CDOM attenuation and (conservative mixing) has been presented in a number of studies (Walsh et al., 2003; Mei et al., 2010; Kowalczuk et al., 2006; Stedmon and Markager, 2003; Højerslev et al., 1996). For instance, such relationships has been applied to represent variable K_{bg} in some coastal and shelf ecosystem models (Walsh et al., 2003; Mei et al., 2010). On the West Florida Shelf, Walsh et al. (2003) found this negative correlation between CDOM attenuation and salinity to be $K_{bg} = 3.470 - 0.095 \times S$ for $S < 28$, $K_{bg} = 0.870 - 0.083 \times S$ for $24 < S < 28$, and $K_{bg} = 2.250-0.060 \times S$ for $S < 24$. While Mei et al. (2010) found the relationship to be $K_{bg}= 0.5352 - 0.001392 \times S$ for $S < 27$ and $K_{bg} = 0.9823 - 0.02995 \times S$ for $S > 27$ in the Gulf of St. Lawrence on the east coast of Canada. In my study K_{bg} was assumed to be determined by two water masses; oceanic water (NAW) and freshwater (FW), and the respecting non-phytoplankton attenuations, K_{NAW} and K_{FW}, corresponding to $K_{bg} = 1.47-0.041 \times S$ (Aksnes, 2015). The approach in my study appears to be relevant also for other coastal waters, although the actual effect on light attenuation varies upon the freshwater substances between locations.

The purpose of comparing simulations to observations was not based on fitting the simulated results to the observations, but rather setting the background attenuation in accordance with the NCW salinity proxy (Eq. 9) for each fjord and setting the turbulent diffusivity (κ) according to the observed differences in stratification for each fjord (section 2.3.1). The simulation model of Huisman et al. (2006) seems to roughly

recreate the vertical structure observed in the three fjords and is therefore used to look at the effect of possible changes in the NCW in general.

Long-term changes in temperature, salinity and density during summer

Temporal trends in temperature and salinity at two of the permanent IMR coastal stations, allowed me to collect information about changes in salinity and temperature back to 1935 and 1942 until 2012 at Sognesjøen and Lista, respectively. A linear regression analysis of temperature versus time at depths of 10 and 50 meters for station Lista provided significant *p*-values (Fig. 6). The slope of the regression lines for temperature also suggested that the temperature has increased over the time period from 1942 to 2012. The slope of the regression lines for salinity was negative, suggesting a decrease in salinity over the same period. However, the linear regression analysis of changes in salinity only came out significant at a 10 m depth. The slopes of the regression lines for density were both negative, suggesting a decrease in density at both 10 and 50 m from 1942 to 2012 at Lista. A linear regression analysis made of temperature versus time at depths of 10 and 50 m at station Sognesjøen, also indicated significant *p*-values (Fig 7). The slope of the regression lines for temperature was positive, suggesting an increased temperature from 1935 to 2012 at this station as well. A linear regression analysis of salinity and of density versus time at depths of 10 and 50 meters for station Sognesjøen provided no significant *p*-values.

A decrease in summertime salinity from the past to the present was implied at station Lista. It has also been suggested that the basin water of some fjords containing NCW has darkened as a result of NCW freshening at a time of year (spring) when the basin waters are renewed (Aksnes et al., 2009). Such freshening i.e. lower salinity was linked to increased precipitation and runoff in Northern Europe, along with increased westerly winds (Sætre, 2007). The data from the two coastal stations suggest that this freshening is less clear during a summer situation. This can be associated with a redistribution of a large fraction of the summer flood to the winter season due to hydroelectric power production (Sjøtun et al., 2015; Opdal et al., 2013).

In section 3.4, the approximated background attenuation for the past scenario (Fig.11A) was higher than the approximated K_{bg} for the present scenario (Fig. 11B) in

Sognesjøen. This did not coincide with that of Lista, where the approximated K_{bg} was lower in the past than in the present. With this in mind, I averaged the salinity down to 25 m in the past (1935) and down to 30 m in the present (2010) in Sognesjøen (there were no salinity measurements at 30 m in 1935). These values suggested an increase in salinity corresponding to a mean salinity of 30.1 ‰ and 32.1 ‰ in 1935 and 2010, respectively. In addition to annual variations, which are large, another potential explanation of salinity changes in Sognefjorden might be due to hydroelectric power plants and water regulation as mentioned above. Several hydroelectric power plants have been developed in Sognesjøen after 1935, and one of the most discussed change mechanisms associated with hydropower development are changes in seasonal patterns (Opdal et al., 2013). The effect of hydropower regulation on salinity, however, requires more in-depth research.

A difference in the mean salinity down to 30 m was observed between the two coastal stations in the present scenario (2010), corresponding to a mean salinity of 32.1 ‰ and 31.2 ‰ in Sognesjøen and Lista, respectively. Although the local runoff situation and annual variation are important it is likely that the observed difference in mean salinity between the two locations is due the location of the stations, i.e. that the salinity within NCC gradually increases northward along the coast as it mixes with the North Sea and the NAW (Sætre, 2007).

The regression lines for density at both 10 and 50 m at Lista are negative, suggesting a decrease in density from the past to the present (Fig. 6) (there were no significant *p*-values of density at Sognesjøen). Density of water is a function of temperature and salinity. Hence, an increased temperature and a decreased salinity will result in a lowered water density. The density change was greater at 10 m than at 50 m thus resulting in stronger stratification over time. One concern of such stronger density stratification is decreased turbulent diffusivities (Denman and Gargett, 1983), reduction of nutrient supply into the euphotic zone (due to lower vertical mixing) (Sarmiento et al., 2004), and consequently reduced phytoplankton production (Boyce et al., 2010). Huisman et al. (2006) discussed the effects of a stronger stratification and lower turbulent diffusivity, and demonstrated that a turbulent diffusivity below 5×10^{-5} m^2s^{-1} would generate oscillation and chaos in the deep chlorophyll maximum (DCM). The approximated turbulent diffusivities for the three fjord locations were

below this threshold (Table 2). For the future scenario at Lista (Table 6), the approximated turbulent diffusivity, i.e. $\kappa = 3.87\times10^{-5}$ m^2 s^{-1} was also below this threshold.

The effect of CDOM attenuation on NCW euphotic zone properties

If the CDOM content of freshwater (FW) and NAW mixes conservatively as indicated by Højerslev et al. (1996) and Kowalczuk et al. (2006) (and assumed in Aksnes, 2015), its absorption will vary linearly with salinity. The background attenuation for NCW used in my simulations was calculated directly from salinity i.e. salinity was used as a proxy for K_{bg} (see section 2.3.1). The idea of conservative mixing goes way back (Figs. 5 and 6 in Højerslev et al., 1996). Højerslev et al. (1996) found the assumption of conservative mixing between the Central North Sea/Atlantic, Baltic Sea and German Bight to be reasonably justified. He also emphasized that the local supply of CDOM needed to be taken into consideration, as variation in CDOM sources or sinks potentially lead to a deviation from the conservative mixing line (Højerslev et al., 1996; del Vecchio and Blough, 2006).

The reciprocal Secchi depth is proportional to the sum of the two attenuation coefficients (c + K) as shown in Eq. (14) (Preisendorfer, 1986). I assumed that K varied in proportion to c + K and on this basis, Secchi depth observations from the Baltic Sea (Fleming-Lehtinen and Laamanen, 2012) were used as a proxy for the change in K_{FW} for the past scenario (Eq. 16). Dissolved organic carbon (DOC) is highly correlated with CDOM (Tranvik, 1990; Thrane et al., 2014). From this, the prediction of elevated OC in the future (Larsen et al., 2011a) was used as a proxy for K_{FW} in a future 1 and future 2 scenario (Eq. 17 and 18, respectively). Note, these proxies are quite different, and consequently both involve uncertainties; The Secchi depth study used for the approximation only addressed the Secchi depth in some sub-regions of the Baltic Sea. Secchi depth shoaling has also been reported in other regions of the Baltic Sea (Sanden and Håkansson, 1996) and in the North Sea (Dupont and Aksnes, 2013). Consequently, relying solely on one study for the Secchi depth proxy may be biased. Secchi depth is also related to the total light attenuation in the water (K) and the beam attenuation coefficient, i.e. not only to the background

attenuation. I also assumed that the CDOM attenuation will change to the same extent as organic carbon in the future (Larsen et al., 2011a) . Even though CDOM and organic carbon are highly correlated (Tranvik, 1990), only 30 to 50 % of the dissolved organic carbon have been suggested to account for CDOM (Thurman et al., 1982). Although I did not use the absolute concentration of OC as basis for increasing future K_{FW}, but rather increased present K_{FW} in proportion with the predicted increase in OC. The connection between OC and K_{FW} is uncertain.

The results from the simulations are consistent with the observed Secchi depth shoaling from the past to the present. Further, for a simulated future scenario with an elevated K_{bg}, the Secchi depth is expected to decrease even more. Results from the simulations indicate a Secchi depth shoaling of approximately 2.5 m at stations Lista and Sognesjøen during the period 2010–2100, i.e. from the present to the future scenario (Table 3 and 4, section 3.3). The Secchi depth shoaling observed in the past, however, might have been caused by other factors than change in K_{bg}, e.g. by an elevated concentration of phytoplankton in the water column during summer time (Sanden and Håkansson, 1996; Fleming-Lehtinen and Laamanen, 2012). However, studies have shown that for many coastal waters, phytoplankton alone is not a good predictor of light attenuation, and that the effect of variation in CDOM (i.e. K_{bg}) is often considered to be of greater significance than phytoplankton (Branco and Kremer, 2005; Kowalczuk et al., 2006; Fleming-Lehtinen and Laamanen, 2012).

Results from the simulations of a future scenario, with an elevated K_{bg}, suggest a 5-meter reduction in the euphotic depth from the present to the future, indicating a shallower euphotic zone at stations Lista and Sognesjøen in the future (Table 3 and 4). A reduced nutricline depth (Z_N) was also observed from the present to the future scenario at both stations, i.e. 5 and 4 m reduction at Lista and Sognesjøen, respectively. Both the surface integrated biomass and primary production also declined from the present to the future. The average nutrient concentration in the upper 20 m (SumN), however, increased with higher K_{bg}. This corresponds to the findings of Urtizberea et al. (2013) who also suggested that an increased nutrient concentration in the euphotic zone due to an elevated K_{bg} resembles that of eutrophication. This will be further discussed below.

In respect to the very different proxies that have been used (i.e. Secchi versus OC), the results showed that the estimated changes in the euphotic zone properties, i.e. expressed as change per year, was greater for a future scenario than those estimated for the past. E.g. an estimated change in the euphotic depth at Lista was 0.02 m y^{-1} and 0.06 m y^{-1} for the past and future scenario, respectively (Table 3).

The effect of changes in vertical diffusivity versus variations in background attenuation

Urtizbera et al. (2013) found that the deep chlorophyll maximum (DCM) depth, i.e. the depth where the simulated phytoplankton abundance was maximal, was much more sensitive to a change in the background attenuation than to the same relative change in the turbulent diffusivity. The changes I estimated in stratification and consequently turbulent diffusivity did not affect the euphotic zone properties to a large extent. E.g. from the simulations of a future scenario at Lista using constant turbulent diffusivity (Table 3), to a future scenario at Lista changing only the turbulent diffusivity (Table 6), the euphotic depth changed from 11.9 to 12.5 m, the Secchi depth changed from 4.5 to 4.9 m and the nutricline depth changed from 10 to 11 m, respectively.

The relative change in turbulent diffusivity was (-) 25%, and the relative change in K_{bg} was 56 % from the present to the future scenario at Lista (Table 6). The relative change from the present to the future scenario in Sognesjøen was (-) 8 % and 54 % for κ and K_{bg}, respectively (Table 8). Thus the relative change was highest for K_{bg}.

Comparing the simulation of a past scenario at station Sognesjøen using a constant κ (Table 3) with the simulation using varied κ (Table 8) showed major differences in the vertical structure of nutrients and phytoplankton and the associated euphotic zone properties. This was due to a higher approximated background attenuation coefficient in the simulation rather than to the change in turbulent diffusivity. The high K_{bg} was due to the slightly lower mean salinity observed in 1935 than in 2010 in Sognesjøen. When I changed only the vertical diffusivity (not shown), however, the euphotic zone properties changed only slightly (i.e. a 3.5 % change in the euphotic depth).

Predicted variations in euphotic, Secchi and nutricline depth as a function of salinity

In Fig.12, the euphotic depth, Secchi depth and the nutricline depth were simulated for the past, present and future scenarios as a function of salinity whose range was set to span from 24 to 35.

The sensitivity analysis demonstrates that the euphotic depth, Secchi depth and nutricline depth decreases from the past to a future scenario, particularly in the salinity range from 24 to 33. The biggest changes (in meters) were observed for salinities between 34 and 35 i.e. where the approximated background attenuation was the lowest, corresponding to K_{NAW}= 0.03 m^{-1}. This is in line with Urtizberea et al. (2013), who suggested that euphotic zone properties are highly sensitive to variation in CDOM attenuation occurring in coastal waters.

Effects of darker coastal water due to increased K_{bg}

Urtizberea et al. (2013) suggested that an increased K_{bg} as a result of elevated CDOM loads causes symptoms that are similar to those associated with eutrophication, such as higher phytoplankton concentration, reduced visibility, and higher nutrient concentration in the upper part of the water column. Such symptoms were also observed in my simulations. From Fig. 8 and 9 one can see that the DCM depth has moved upwards from the past to a future scenario, i.e. as K_{bg} was increased. My results also showed that the total phytoplankton biomass of the euphotic zone has decreased from the past to the future scenario (Table 3 and 4). This was also addressed in Mellard et al. (2011), who found that an elevated CDOM attenuation increases the light limitation, and consequently shifts the vertical distribution of phytoplankton upwards in the water column, and decreases the total phytoplankton mass. It should be noted, however, despite the decreased total phytoplankton biomass and production in the future scenario, that the phytoplankton concentration of the uppermost part of the water increased due to the upward shift. This also makes the Secchi depth shallower which is indicative for eutrophication although the simulated water column indeed became more oligotrophy in the present scenario. Further, the simulation showed that also the nutricline depth has been “lifted” towards the surface

in a future scenario, and that the sum of nutrients (nitrate) in the upper 20 m has increased due to higher CDOM attenuation (Table 3 and 4). Such simulated "lift" of nutrients toward the surface is due to the reduced nitrate consumption as a consequence of reduced light penetration at depth due to elevated background attenuation, and also a result of more self-shading from elevated phytoplankton concentration in the upper part of the water column (Urtizberea et al., 2013)

A Secchi depth shoaling has been observed in the Baltic- and the North Sea the last hundred years (Dupont and Aksnes, 2013; Fleming-Lehtinen and Laamanen, 2012; Sanden and Håkansson, 1996). Since elevated K_{bg} is linked to increased CDOM loads in my study, my simulations suggest that the Secchi depth will continue to decrease in the future. Secchi depth shoaling is associated with an increase in the beam attenuation coefficient (c), and the vertical attenuation coefficient (K) (Eq. 14) (Preisendorfer, 1986). However, it is not possible to differentiate between the contributions of the two for a certain Secchi depth observation. Elevated attenuation (K) implies shoaling and narrowing of the vertical habitat for organisms that have a preferred range of light intensity, whereas an increase in c reduces the sighting distance for an organism that utilize vision in their search for prey, e.g. fish (Dupont and Aksnes, 2013).

Reduced light penetration, and consequently a euphotic depth shoaling, has also been suggested to bring about a decrease in the depth limit of algae. Rueness and Fredriksen (1991) reported a decrease in a number of common algal species in the outer Oslofjord from around 1950 to 1989. At the same time the depth limit of algal vegetation was shown to have moved significantly upward. Further, the sugar kelp (*Saccharina latissima*) has disappeared from large areas of the Skagerrak coast, and the prevalence along the southwest coast of Norway has been reduced (Moy et al., 2008). The lower limit of bladder wrack (*Fucus vesiculosus*) has also been reported moving upward from 11.5 m in 1943/1944 to 8.5 m in 1984 in the outer archipelago of the Åland Sea (Kautsky et al., 1986). This illustrates that the light penetration (i.e. K) is an important determinant for the depth distribution of benthic algae. From my simulations, increased K_{bg} associated with CDOM predicts a shallower euphotic zone in the future from 17 to 12 m from the present to the future scenario at Lista (Table 3) and from 18 to 13 m from the present to the future scenario in Sognesjøen (Table 4).

This may be of concern, not only for the phytoplankton, but also for the benthic algal distribution in the future.

Thrane et al. (2014) suggested that a future scenario with increased CDOM in boreal lakes could also negatively affect the primary production. This corresponds to my results, where the surface integrated primary production decreased with an increasing $K_{bg.}$ The surface integrated primary production decreased by 10% from the present to the future scenario at Lista (Table 3). In Sognesjøen the surface integrated primary production decreased by 9 % from the present to the future scenario (Table 4).
Note, however, that my future and past scenario simulations do not account for changes in nutrient supplies due to human activity. Human activities, such as burning fossil fuels and application of nitrogen-based fertilizers, have significant impact on the amount of nitrogen that is available in an ecosystem (Bernhard, 2012). However, as a result of emission standards and regulations, such emissions might be less in the future. Anthropogenic nitrogen emissions has additionally been suggested to steer to anoxia or hypoxia, altered biodiversity, changes in food-web structure, and habitat degradation (Bernhard, 2012).

Conclusion

My results are consistent with observed Secchi depth shoaling from the past to the present. Such shoaling was also observed for both the euphotic depth and nutricline depth. This suggests that a change in the euphotic habitat, due to CDOM attenuation, has already occurred from the past to the present. The estimated changes in the NCW euphotic zone properties, however, are suggested to be greater in the future than those estimated for the past. This is based on increased supplies of terrestrial OC in the future, and Secchi depth observation from the past. From this, an elevated CDOM attenuation due to increased supplies of terrestrial OC is likely to cause a more pronounced shoaling and narrowing of the NCW euphotic habitat in the future. Further, my results suggest that an elevated CDOM attenuation in the future may show similar symptoms as the effect of eutrophication, i.e. cause a shift of the vertical distributions of phytoplankton and nutrient toward the surface, reduced visibility (due to euphotic zone compression and higher phytoplankton density), and higher nutrient

concentration in the upper water column. However, the simulations also indicated lower primary production which means more oligotrophy rather than eutrophy. Further, my results suggest that while the NCW euphotic zone properties are susceptible to future increase in CDOM attenuation, they are to a lesser degree susceptible to a potential increase in density stratification (in line with Urtizbera et al., 2013). Shoaling and narrowing of the euphotic habitat due to increased light absorption associated with elevated CDOM concentration, and also due to higher concentrations of phytoplankton in the surface water, may provide major implications on the biological community.

5 REFERENCES

AKSNES, D. L. 2015. Sverdrup critical depth and the role of water clarity in Norwegian Coastal Water. *Ices Journal of Marine Science,* 72**,** 2041-2050.

AKSNES, D. L., DUPONT, N., STABY, A., FIKSEN, XD, KAARTVEDT, S. & AURE, J. 2009. Coastal water darkening and implications for mesopelagic regime shifts in Norwegian fjords. *Marine Ecology Progress Series,* 387**,** 39-49.

AKSNES, D. L. & LIE, U. 1990. A coupled physical-biological pelagic model of a shallow sill fjord. *Estuarine, Coastal and Shelf Science,* 31**,** 459-486.

AKSNES, D. L., MAGNESEN, T. & LIE, U. 1985. Nutrient enrichment experiments in plastic cylinders and the implications of enhanced primary production in Lindåspollene, western Norway. *Sarsia,* 70**,** 45-58.

AKSNES, D. L., OHMAN, M. D. & RIVIERE, P. 2007. Optical effect on the nitracline in a coastal upwelling area. *Limnology and oceanography,* 52**,** 1179-1187.

AURE, J., DANIELSSEN, D. & SAETRE, R. 1996. Assessment of eutrophication in Skagerrak coastal waters using oxygen consumption in fjordic basins. *Ices Journal of Marine Science,* 53**,** 589-595.

BERNHARD, A. 2012. The nitrogen cycle: Processes, players, and human impact. *Nature Education Knowledge,* 3**,** 25.

BOYCE, D. G., LEWIS, M. R. & WORM, B. 2010. Global phytoplankton decline over the past century. *Nature,* 466**,** 591-596.

BRANCO, A. B. & KREMER, J. N. 2005. The relative importance of chlorophyll and colored dissolved organic matter (CDOM) to the prediction of the diffuse attenuation coefficient in shallow estuaries. *Estuaries,* 28**,** 643-652.

BRICAUD, A., BABIN, M., MOREL, A. & CLAUSTRE, H. 1995. Variability in the chlorophyll-specific absorption coefficients of natural phytoplankton: Analysis and parameterization. *Journal of Geophysical Research: Oceans,* 100**,** 13321-13332.

CARDER, K. L., STEWARD, R. G., HARVEY, G. R. & ORTNER, P. B. 1989. Marine Humic and Fulvic-Acids - Their Effects on Remote-Sensing of Ocean Chlorophyll. *Limnology and Oceanography,* 34**,** 68-81.

DEL VECCHIO, R. & BLOUGH, N. V. 2006. Influence of Ultraviolet Radiation on the Chromophoric Dissolved Organic Matter in Natural Waters. *In:* GHETTI, F., CHECCUCCI, G. & BORNMAN, J. F. (eds.) *Environmental UV Radiation: Impact on Ecosystems and Human Health and Predictive Models: Proceedings of the NATO Advanced Study Institute on Environmental UV Radiation: Impact on Ecosystems and Human Health and Predictive Models Pisa, Italy June 2001.* Dordrecht: Springer Netherlands.

DENMAN, K. L. & GARGETT, A. E. 1983. Time and space scales of vertical mixing and advection of'phytoplankton in the upper ocean. *Oceanography,* 28.

DUPONT, N. & AKSNES, D. L. 2013. Centennial changes in water clarity of the Baltic Sea and the North Sea. *Estuarine, Coastal and Shelf Science,* 131**,** 282-289.

ERGA, S. R. 1989a. Ecological studies on the phytoplankton of Boknafjorden, Western Norway. 1. The effect of water exchange processes and environmental factors on temporal and vertical variability of biomass. *Sarsia,* 74**,** 161-176.

ERGA, S. R. 1989b. Ecological studies on the phytoplankton of Boknafjorden, western Norway. II. Environmental control of photosynthesis. *Journal of Plankton Research,* 11**,** 785-812.

ERGA, S. R. & SKJOLDAL, H. R. 1990. Diel variations in photosynthetic activity of summer phytoplankton in Lindåspollene, western Norway.

ERGA, S. R., SSEBIYONGA, N., FRETTE, Ø., HAMRE, B., AURE, J., STRAND, Ø. & STROHMEIER, T. 2012. Dynamics of phytoplankton distribution and photosynthetic capacity in a western Norwegian fjord during coastal upwelling: effects on optical properties. *Estuarine, Coastal and Shelf Science,* 97**,** 91-103.

EVANS, C. D., MONTEITH, D. T. & COOPER, D. M. 2005. Long-term increases in surface water dissolved organic carbon: Observations, possible causes and environmental impacts. *Environmental Pollution,* 137**,** 55-71.

FINSTAD, A. G., ANDERSEN, T., LARSEN, S., TOMINAGA, K., BLUMENTRATH, S., DE WIT, H. A., TOMMERVIK, H. & HESSEN, D. O. 2016. From greening to browning: Catchment vegetation development and reduced S-deposition promote organic carbon load on decadal time scales in Nordic lakes. *Sci Rep,* 6**,** 31944.

FLEMING-LEHTINEN, V. & LAAMANEN, M. 2012. Long-term changes in Secchi depth and the role of phytoplankton in explaining light attenuation in the Baltic Sea. *Estuarine, Coastal and Shelf Science,* 102**,** 1-10.

FRIGSTAD, H., ANDERSEN, T., HESSEN, D. O., JEANSSON, E., SKOGEN, M., NAUSTVOLL, L.-J., MILES, M. W., JOHANNESSEN, T. & BELLERBY, R. G. J. 2013. Long-term trends in carbon, nutrients and stoichiometry in Norwegian coastal waters: Evidence of a regime shift. *Progress in Oceanography,* 111**,** 113-124.

GREENE, C. H., PERSHING, A. J., CRONIN, T. M. & CECI, N. 2008. Arctic Climate Change and Its Impacts on the Ecology of the North Atlantic. *Ecology,* 89**,** S24-S38.

HJORT, J. & GRAN, H. H. 1899. Currents and pelagic life in the Northern Ocean. *Report on Norwegian FIshery and Marine Investigations 1895-1897. Bergen Museums Skrifter,* 6**,** 1-24.

HUISMAN, J., PHAM THI, N. N., KARL, D. M. & SOMMEIJER, B. 2006. Reduced mixing generates oscillations and chaos in the oceanic deep chlorophyll maximum. *Nature,* 439**,** 322-5.

HØJERSLEV, N. K., HOLT, N. & AARUP, T. 1996. Optical measurements in the North Sea-Baltic Sea transition zone. I. On the origin of the deep water in the Kattegat. *Continental Shelf Research,* 16**,** 1329-1342.

IMR. 2013. *The Norwegian Coastal Current* [Online]. Institute of Marine Research: . Available: http://www.imr.no/temasider/kyst_og_fjord/den_norske_kyststrommen/en.

KAISER, M. J., ATTRILL, M. J., JENNINGS, S., THOMAS, D. D., BARNES, D. K. A., BRIERLEY, A. S., HIDDINK, J. G., KAARTOKALLIO, H., POLUNIN, N. V. C. & RAFFAELI, D. G. 2011. *Marine ecology : processes, systems, and impacts,* Oxford ; New York, Oxford University Press.

KAUTSKY, N., KAUTSKY, H., KAUTSKY, U. & WAERN, M. 1986. Decreased depth penetration of Fucus vesiculosus (L.) since the 1940's indicates eutrophication of the Baltic Sea. *Mar. Ecol. Prog. Ser,* 28**,** 1-8.

KIRK, J. T. O. 2011. *Light and photosynthesis in aquatic ecosystems,* Cambridge, UK ; New York, Cambridge University Press.

KOWALCZUK, P., A. STEDMON, C. & MARKAGER, S. 2006. Modeling absorption by CDOM in the Baltic Sea from season, salinity and chlorophyll. *Marine Chemistry,* 101**,** 1-11.

KOWALCZUK, P., COOPER, W. J., WHITEHEAD, R. F., DURAKO, M. J. & SHELDON, W. 2003. Characterization of CDOM in an organic-rich river and surrounding coastal ocean in the South Atlantic Bight. *Aquatic Sciences,* 65**,** 384-401.

KOWALCZUK, P., STON-EGIERT, J., COOPER, W. J., WHITEHEAD, R. F. & DURAKO, M. J. 2005. Characterization of chromophoric dissolved organic matter (CDOM) in the Baltic Sea by excitation emission matrix fluorescence spectroscopy. *Marine Chemistry,* 96**,** 273-292.

LARSEN, S., ANDERSEN, T. & HESSEN, D. O. 2011a. Climate change predicted to cause severe increase of organic carbon in lakes. *Global Change Biology,* 17**,** 1186-1192.

LARSEN, S., ANDERSEN, T. & HESSEN, D. O. 2011b. Predicting organic carbon in lakes from climate drivers and catchment properties. *Global Biogeochemical Cycles,* 25.

LAVIGNE, H., D'ORTENZIO, F., MIGON, C., CLAUSTRE, H., TESTOR, P., D'ALCALÀ, M. R., LAVEZZA, R., HOUPERT, L. & PRIEUR, L. 2013. Enhancing the comprehension of mixed layer depth control on the Mediterranean phytoplankton phenology. *Journal of Geophysical Research: Oceans,* 118**,** 3416-3430.

LEE, Z., WEIDEMANN, A., KINDLE, J., ARNONE, R., CARDER, K. L. & DAVIS, C. 2007. Euphotic zone depth: Its derivation and implication to ocean-color remote sensing. *Journal of Geophysical Research: Oceans,* 112**,** n/a-n/a.

LEENHEER, J. A. & CROUE, J. P. 2003. Characterizing aquatic dissolved organic matter. *Environmental Science & Technology,* 37**,** 18A-26A.

MANNINO, A., RUSS, M. E. & HOOKER, S. B. 2008. Algorithm development and validation for satellite-derived distributions of DOC and CDOM in the U.S. Middle Atlantic Bight. *Journal of Geophysical Research: Oceans,* 113.

MEI, Z.-P., SAUCIER, F. J., LE FOUEST, V., ZAKARDJIAN, B., SENNVILLE, S., XIE, H. & STARR, M. 2010. Modeling the timing of spring phytoplankton bloom and biological production of the Gulf of St. Lawrence (Canada): effects of colored dissolved organic matter and temperature. *Continental Shelf Research,* 30**,** 2027-2042.

MELLARD, J. P., YOSHIYAMA, K., LITCHMAN, E. & KLAUSMEIER, C. A. 2011. The vertical distribution of phytoplankton in stratified water columns. *Journal of Theoretical Biology,* 269**,** 16-30.

MOLVÆR, J., EIKREM, W., MAGNUSSON, J., PEDERSEN, A. & TJOMSLAND, T. 2007. Common Procedure for Identification of the Eutrophication Status of Maritime Area of the Oslo and Paris Conventions. Report on the Eutrophication Status for the Norwegian Skagerrak Coast.

MONAHAN, E. C. & PYBUS, M. J. 1978. Color, Ultraviolet Absorbance and Salinity of Surface Waters Off West-Coast of Ireland. *Nature,* 274**,** 782-784.

MONIN, A. S. 1990. *Theoretical geophysical fluid dynamics,* Dordrecht ; Boston, Kluwer Academic Publishers.

MOREL, A. & MARITORENA, S. 2001. Bio-optical properties of oceanic waters- A reappraisal. *Journal of Geophysical research,* 106**,** 7163-7180.

MOY, F., CHRISTIE, H., STTEN, H., STÅLNACKE, P., AKSNES, D., ALVE, E., AURE, J., BEKKBY, T., FREDRIKSEN, S., GITMARK, J., HACKETT, B., MAGNUSSON, J., PENGERUD, A., SJØTUN, K., SØRENSEN, K., TVEITEN, L., ØYGARDEN, L. & ÅSEN, P. A. 2008. *Sluttrapport fra Sukkertareprosjektet 2005-2008. Final report from the Sugar Kelp Project 2005-2008,* Oslo, NIVA.

NELSON, N. B. & SIEGEL, D. A. 2013. The global distribution and dynamics of chromophoric dissolved organic matter. *Annual Review of Marine Science,* 5**,** 447-476.

OMAND, M. M. & MAHADEVAN, A. 2015. The shape of the oceanic nitracline.

OPDAL, A. F., AKSNES, D. L., ROSLAND, R. & FIKSEN, Ø. 2013. Sognefjorden - en oppsummering av litteratur og kunnskapsstatus om fjordøkologi og vannkraftutbygging. Kunnskapsinnhenting. *Uni Research***,** 1-40.

PASQUERON DE FOMMERVAULT, O., D'ORTENZIO, F., MANGIN, A., SERRA, R., MIGON, C., CLAUSTRE, H., LAVIGNE, H., RIBERA D'ALCALÀ, M., PRIEUR, L. & TAILLANDIER, V. 2015. Seasonal variability of nutrient concentrations in the Mediterranean Sea: Contribution of Bio-Argo floats. *Journal of Geophysical Research: Oceans*.

PREISENDORFER, R. W. 1986. SECCHI DISK SCIENCE - VISUAL OPTICS OF NATURAL-WATERS. *Limnology and Oceanography,* 31**,** 909-926.

PAASCHE, E. & ERGA, S. R. 1988. Phosphorus and nitrogen limitation of phytoplankton in the inner Oslofjord (Norway). *Sarsia,* 73**,** 229-243.

ROULET, N. & MOORE, T. R. 2006. Environmental chemistry: browning the waters. *Nature,* 444**,** 283-284.
RUENESS, J. & FREDRIKSEN, S. 1991. An assessment of possible pollution effects on the benthic algae of the outer Oslofjord, Norway. *Oebalia. Taranto,* 17.
SANDEN, P. & HÅKANSSON, B. 1996. Long-term trends in Secchi depth in the Baltic Sea. *Limnology and Oceanography,* 41**,** 346-351.
SARMIENTO, J. L. & GRUBER, N. 2006. *Ocean Biogeochemical Dynamics*, Princeton University Press.
SARMIENTO, J. L., GRUBER, N., BRZEZINSKI, M. A. & DUNNE, J. P. 2004. High-latitude controls of thermocline nutrients and low latitude biological productivity. *Nature,* 427**,** 56-60.
SCHULTEN, H. R., PLAGE, B. & SCHNITZER, M. 1991. A Chemical-Structure for Humic Substances. *Naturwissenschaften,* 78**,** 311-312.
SJØTUN, K., HUSA, V., ASPLIN, L. & SANDVIK, A. D. 2015. Climatic and environmental factors influencing occurrence and distribution of macroalgae - a fjord gradient revisited. *Marine Ecology Progress Series,* 532**,** 73-88.
SORTEBERG, A. 2014. Nedbør i Norge siden 1900. *Naturen,* 138**,** 221-231.
STEDMON, C. A. & MARKAGER, S. 2003. Behaviour of the optical properties of coloured dissolved organic matter under conservative mixing. *Estuarine, Coastal and Shelf Science,* 57**,** 973-979.
STEDMON, C. A., OSBURN, C. L. & KRAGH, T. 2010. Tracing water mass mixing in the Baltic–North Sea transition zone using the optical properties of coloured dissolved organic matter. *Estuarine, Coastal and Shelf Science,* 87**,** 156-162.
SVERDRUP, H. U., JOHNSON, M. W. & FLEMING, R. H. 1942. *The Oceans: Their physics, chemistry, and general biology*, Prentice-Hall New York.
SÆTRE, R. 2007. *The Norwegian coastal current : oceanography and climate,* Trondheim, Tapir Academic Press.
SÆTRE, R. & LJØEN, R. 1972. The Norwegian coastal current.
SØRNES, T. A. & AKSNES, D. L. 2006. Concurrent temporal patterns in light absorbance and fish abundance. *Marine Ecology Progress Series,* 325**,** 181-186.
THRANE, J. E., HESSEN, D. O. & ANDERSEN, T. 2014. The Absorption of Light in Lakes: Negative Impact of Dissolved Organic Carbon on Primary Productivity. *Ecosystems,* 17**,** 1040-1052.
THURMAN, E. M., WERSHAW, R. L., MALCOLM, R. L. & PINCKNEY, D. J. 1982. Molecular size of aquatic humic substances. *Organic Geochemistry,* 4**,** 27-35.
TRANVIK, L. J. 1990. Bacterioplankton Growth on Fractions of Dissolved Organic-Carbon of Different Molecular-Weights from Humic and Clear Waters. *Applied and Environmental Microbiology,* 56**,** 1672-1677.
URTIZBEREA, A., DUPONT, N., ROSLAND, R. & AKSNES, D. L. 2013. Sensitivity of euphotic zone properties to CDOM variations in marine ecosystem models. *Ecological Modelling,* 256**,** 16-22.

WALSH, J. J., WEISBERG, R. H., DIETERLE, D. A., HE, R., DARROW, B. P., JOLLIFF, J. K., LESTER, K. M., VARGO, G. A., KIRKPATRICK, G. J. & FANNING, K. A. 2003. Phytoplankton response to intrusions of slope water on the West Florida Shelf: Models and observations. *Journal of Geophysical Research: Oceans,* 108.

6 APPENDIX

A Matlab codes

The original-and modified simulation model of Huisman et al. (2006) was programmed in MATLAB R2015b, and the following codes formed the basis of the analyses in this study.

A1 The simulation model of Huisman et al. (2006)

```
%Huisman_model. Phytoplankton model as in Huisman et al.(2006).
%Programmed 160115 DL Aksnes. Modified by Erik

clear all

% Temporal and spatial discretization
Z=300;          % Number of depth cells
DZ=1;           % Length of a depth cell (m)
%T=345600;      % Number of time steps - duration corresponds to fig 2c
                % in Huisman
DT=300;         % Length of a time step(s)
T = 120000;     % Number of time steps

%Water column properties - constant coefficients as in Huisman et
%al.(2006)

kappa=1.2E-5; % Turbulent diffusivity (m2 s-1)(Note that Huisman uses
              % cm2 s-1)
I0=600;         % Irradiance at surface (mmol photons m-2 s-1)
Kb=0.045;       % Background light attenuation (m-1)
NB=10;          % Fixed nutrient concentration in last depth cell (mmol
                % N m-3)

%Phytoplankton traits as in Huisman et al (2006)

alfa=1E-9;      % Nutrient content of a phytoplankton cell (mmol N
cell^-1)
umax=1.11E-5; % Max growth rate (s-1)
m=2.78E-6;      % loss (death)rate (s-1)
Hi=20;          % Half saturation irradiance (micromol photons m-2 s-1)
Hn=0.025;       % Half saturation nutrient (mmol m-3)
Kp=0.6;         % Specific light attenuation of phytoplankton
(m^2(mmolN)^-1)
                % OBS: This coefficient is 6E-10 m2 cell-1 in Huisman
as
                % their phytoplankton state variable is specified in
                % units of cells. Here the unit is mmol N.
v=1.17E-5;      % Sinking velocity of phytoplankton (m s-1)
eps=0.5;        % Nutrient recycling coefficient

%Initialization of water column state variables. File 'initialstate'
%contains values close to steady state to minimize runtime.

load('initialstate','nit1','phy1');

%Note that both nutrients (nit1) and phytoplankton (phy1) are given
```

```
in %units of mmol N m-3 (Phytoplankton is given in units of cells m-
3 in
%Huisman et al

%Coefficients that specify relative exchanges between depth cells
%during a time step
S1=kappa*DT/(DZ*DZ); % the fraction of a depth cell that is
                     % exchanged with the neighbour cells due to
                     % turbulent diffusivity
R2=v*DT/DZ;          % The fraction of phytoplankton in a depth cell
                     % that sinks to the cell below during DT

%Assigning values to memory (for increased speed)

K = zeros(1,Z);
Iz = zeros(1,Z);

for tstep=1:T %Time loop

    %Update water column irradiance
    K=Kb+Kp*phy1(1);      % Light attenuation of first depth cell
                          % (surface)
    Iz(1)=I0*exp(-K*DZ/2) % Irradiance in first depth cell (in middle
                          % of cell)

%     for n=2:Z              % Calculate irradiance for all other
                             % depth cells
%         K=Kb+Kp*phy1(n)*DZ;
%         Iz(n)=Iz(n-1)*exp(-K*DZ); %Irradiance - still in middle of
                                    %depth cell
%     end

    K(2:Z)=Kb+Kp*phy1(2:Z);
    Iz(2:Z)=Iz(1:Z-1).*exp(-K(2:Z)*DZ); % Irradiance - still in
                                        % middle of depth cell

    %Update phytoplankton growth and loss terms

%     for n=1:Z
%         Ilim=Iz(n)/(Iz(n)+Hi);     %light limitation of depth cell
%         Nlim=nit1(n)/(nit1(n)+Hn); %nutrient limitation of depth
%                                    %cell
%         u=umax*min(Ilim,Nlim);     %phytoplankton growth rate
%         ST1(n)=u*phy1(n)*DT;       %Growth of phytoplankton during
%                                    %DT
%         ST2(n)=m*phy1(n)*DT;       %Loss of phytoplankton during DT
%     end

     Ilim=Iz./(Iz+Hi);       %light limitation of depth cell
     Nlim=nit1./(nit1+Hn);   %nutrient limitation of depth cell
     u=umax*min(Ilim,Nlim); %phytoplankton growth rate
     ST1=u.*phy1*DT;         %Growth of phytoplankton during DT
     ST2=m*phy1*DT;          %Loss of phytoplankton during DT


    %Update first (surface) depth cell - no exchange through surface
    nit2(1)=nit1(1)*(1-S1)+nit1(2)*S1-ST1(1)+eps*ST2(1);
    phy2(1)=phy1(1)*(1-S1-R2)+phy1(2)*S1+ST1(1)-ST2(1);

    %Update last depth cell. Nutrient concentration is fixed in last
    %cell! Phytoplankton is not transported (by diffusion/sinking)
```

```
    %below the last depth cell.

    nit2(Z)=NB;
    phy2(Z)=phy1(Z)*(1-S1)+phy1(Z-1)*(S1+R2)+ST1(Z)-ST2(Z);

   % Update all the intermediate depth cells
%      for n=2:Z-1
%          nit2(n)=nit1(n)*(1-S1-S1)+nit1(n-1)*S1+nit1(n+1)*S1-
ST1(n)+eps*ST2(n);
%          phy2(n)=phy1(n)*(1-S1-S1-R2)+phy1(n-
1)*(S1+R2)+phy1(n+1)*S1+ST1(n)-ST2(n);
%      end

    nit2(2:Z-1)=nit1(2:Z-1).*(1-S1-S1)+nit1(1:Z-2).*S1+nit1(3:Z)*S1-
ST1(2:Z-1)+eps*ST2(2:Z-1);
    phy2(2:Z-1)=phy1(2:Z-1).*(1-S1-S1-R2)+phy1(1:Z-
2).*(S1+R2)+phy1(3:Z)*S1+ST1(2:Z-1)-ST2(2:Z-1);

    %Store for figures
    nitplot(:,tstep)=nit2(:);
    phyplot(:,tstep)=phy2(:)/alfa; %alfa converts from mmol to cell
                                   %numbers for plotting

    %Proceed to next time step with updated state variables
    nit1=nit2;
    phy1=phy2;
end

% Plot figures

for tstep=1:T
    X(tstep)=tstep*DT/(3600*24);   %Time-axis in days
end

for n=1:Z
    Y(n)=n*DZ;                     %Depth-axis in meters
end

figure(1);
figure1=imagesc(X,Y(70:120),nitplot(70:120,:));
ht=title('Nutrient concentration mmol m-3');
hx=xlabel('Time (days)');
hy=ylabel('Depth (m)');
colorbar

figure(2);
figure2=imagesc(X,Y(70:120),phyplot(70:120,:));
ht=title('Phytoplankton concentration cells m-3');
hx=xlabel('Time (days)');
hy=ylabel('Depth (m)');
colorbar
```

A2 Modified model

```
clear all

% Temporal and spatial discretization
Z=50;         % Number of depth cells
DZ=1;         % Length of a depth cell (m)
DT=300;       % Length of a time step(s)
T = 120000;   % Number of time steps

%Water column properties

kappa=5.18E-5; % Turbulent diffusivity (m2 s-1). This varied
I0=600;        % Irradiance at surface (mmol photons m-2 s-1)
Kb=0.191;      % Background light attenuation (m-1). This varied
NB=15;         % Fixed nutrient concentration in last depth cell
               % (mmol N m^-3)

%Phytoplankton traits

alfa=1E-9;     % Nutrient content of a phytoplankton cell (mmol N
               % cell^-1)
umax=1.11E-5; % Max growth rate (s-1)
m=2.78E-6;     % loss (death)rate (s-1)
Hi=20;         % Half saturation irradiance (micromol photons m-2 s-1)
Hn=0.025;      % Half saturation nutrient (mmol m-3)

K1=0.16;        % Morel & Maritorena (2001) coefficient converted to
                % mmol N m-3 from mg m^-3 (at 440 nm) according to
                % Sarmiento and Gruber (2006)
K2=0.67;        % Morel & Maritorena "raising to a power". Exponent
                % used in the light attenuation equation

v=1.17E-5;     % Sinking velocity of phytoplankton (m s-1)
eps=0.5;       % Nutrient recycling coefficient

%Output values:

Ie=I0/100;      %The downwelling irradiance of PAR falls to 1% of that
                %just below the surface
Cn=7.3;         %C:N ratio (117:16) from Sarmiento & Gruber
Cw=12;          %Molecular weight of Carbon
Cchl=50;        %C:Chl ratio

%Initialization of water column state variables. File 'initialstate'
%contains values close to steady state to minimize runtime.

load('initialstate', 'nit1', 'phy1');

%Note that both nutrients (nit1) and phytoplankton (phy1) are given
in units of mmol N m-3
```

```
%Coefficients that specify relative exchanges between depth cells
%during a time step

S1=kappa*DT/(DZ*DZ); % the fraction of a depth cell that is exchanged
                     % with the neighbor cells due to turbulent
                     % diffusivity
R2=v*DT/DZ;          % The fraction of phytoplankton in a depth cell
                     % that sinks to the cell below during DT

%Assigning values to memory (for increased speed)

K = zeros(1,Z);
Iz = zeros(1,Z);

for n=1:Z
    Y(n)=n*DZ;               %Depth-axis in meters
end


for tstep=1:T %Time loop

    %Update water column irradiance

    K=Kb+K1*phy1(1)^K2;      % Light attenuation of first depth cell
                             % (surface).The light attenuation is
                             % changed to that of Morel &
                             % Maritorena(2001)
    Iz(1)=I0*exp(-K*DZ/2);   % Irradiance in first depth cell (in
                             % middle of cell)
    K(2:Z)=Kb+K1*phy1(2:Z).^K2;  %In correspondance with the "new"
                                 %light attenuation equation
    Iz(2:Z)=Iz(1:Z-1).*exp(-K(2:Z)*DZ); %Irradiance - still in middle
                                        %of depth cell

     %Update phytoplankton growth and loss terms

     Ilim=Iz./(Iz+Hi);           %light limitation of depth cell
     Nlim=nit1./(nit1+Hn);       %nutrient limitation of depth cell
     u=umax*min(Ilim,Nlim);      %phytoplankton growth rate
     ST1=u.*phy1*DT;             %Growth of phytoplankton during DT
     ST2=m*phy1*DT;              %Loss of phytoplankton during DT


    %Update first (surface) depth cell - no exchange through surface

    nit2(1)=nit1(1)*(1-S1)+nit1(2)*S1-ST1(1)+eps*ST2(1);
    phy2(1)=phy1(1)*(1-S1-R2)+phy1(2)*S1+ST1(1)-ST2(1);

    % Update last depth cell. Nutrient concentration is fixed in last
    % cell! Phytoplankton is not transported (by diffusion/sinking)
    % below the last depth cell.
    nit2(Z)=NB;
```

```
    phy2(Z)=phy1(Z)*(1-S1)+phy1(Z-1)*(S1+R2)+ST1(Z)-ST2(Z);


    nit2(2:Z-1)=nit1(2:Z-1).*(1-S1-S1)+nit1(1:Z-2).*S1+nit1(3:Z)*S1-
ST1(2:Z-1)+eps*ST2(2:Z-1);
    phy2(2:Z-1)=phy1(2:Z-1).*(1-S1-S1-R2)+phy1(1:Z-
2).*(S1+R2)+phy1(3:Z)*S1+ST1(2:Z-1)-ST2(2:Z-1);


    %Store for figures
    nitplot(:,tstep)=nit2(:);
    phyplot(:,tstep)=phy2(:)/alfa; %alfa converts from mmol to cell
                                   %numbers for plotting

    %Proceed to next time step with updated state variables
    nit1=nit2;
    phy1=phy2;

    %find euphotic depth (Ze)
    if tstep==(T-105120) %One year equals 105120 timesteps
        n=1;
        Ze= Z*DZ;
        while Y(n)<Ze
            Ks=log(I0/Iz(n))/Y(n);
            Ze=-log(0.01)/Ks;
            n=n+1;
        end %while
        Ze1=Ze
    end %if


end

% Plot figures
for tstep=1:T
    X(tstep)=tstep*DT/(3600*24);   %Time-axis in days
end

figure(1);
figure1=imagesc(X,Y(1:30),nitplot(1:30,:));
ht=title('Nutrient concentration mmol m^{-3}');
hx=xlabel('Time (days)');
hy=ylabel('Depth (m)');
colorbar

figure(2);
figure2=imagesc(X,Y(1:30),phyplot(1:30,:));
ht=title('Phytoplankton concentration cells m^{-3}');
hx=xlabel('Time (days)');
hy=ylabel('Depth (m)');
colorbar
```

```
%Ze is the euphotic zone, i.e. the depth at which the incident light
%is at 1%. Ze is affected by the attenuation coefficient

n=1;
Ze= Z*DZ;
while Y(n)<Ze
    Ks=log(I0/Iz(n))/Y(n);
    Ze=-log(0.01)/Ks;
    n=n+1;
end %while
Ze2=Ze

%Calculate percentage change of euphotic depth. A criteria for the
%steady state

Zechange=100*(Ze2-Ze1)/Ze2

%Zs is the secchi depth. Ks is the attenuation coefficient from the
%surface down to the secchi depth
%Ks=-log(Iz/I0)/Y(n);
%Ks=1.44/Zs--> Zs=1.44/Ks retrieved from Kirk (2011)

Zs=Z*DZ;
n=1;
while Y(n)<Zs
    Ks=-log(Iz(n)/I0)/Y(n);
    Zs=1.44/Ks;
    n=n+1;
end

%%

figure(3);%the vertical distributions of nitrate and phytoplankton
          %in the same plot, but with different scaling (i.e. double
          %axes)
set(gcf,'Name','Nitrate and Phytoplankton')
line(nit1,-Y,'Color','b', 'LineWidth', 1.5)
ax1 = gca; % current axes
ax1.XColor = 'b';
ax1.YColor = 'k';

ax1_pos = ax1.Position;% position of first axes
ax2 = axes('Position',ax1_pos,...
    'XAxisLocation','top','xcolor', [0 .5 0],'YAxislocation',
    'right',...'Color','none');
line(phy1,-Y,'Parent',ax2, 'color', [0 .5 0], 'LineWidth', 1.5)
xlabel(ax1, 'Nitrate (mmol N m^{-3})');
set (ax1,'Xlim', [0 20], 'Xtick', [0:2:20]);
xlabel(ax2, 'Phytoplankton (mmol N m^{-3})');
set (ax2, 'Xlim', [0 1.3], 'Xtick', [0:.1:1.3]);
ylabel(ax1, 'Depth (m)');

%%
```

```
%Total production.
Pi=sum(ST1); % Surface integrated primary production (ST1)
Pi=Pi*(3600)/DT %from mmol N m-2 per dt to mmol N m-2 per hour
%%

%Biomass phytoplankton
Bi=sum(phy1) %Surface integrated biomass mmol N m-2

%%

%Average nutrient concentration in the upper 20 m
SumN = sum(nit1(1:20))/20
```

B Variation in euphotic, Secchi and nutricline depth as a function of salinity

Appendix B, Table 1: Predicted variations in euphotic, nutricline, and Secchi depth as a function of salinity in a gradient from NCW_{24} to NAW_{35} in the past

‰	24	25	26	27	28	29	30	31	32	33	34	35
κ	5.18	5.18	5.18	5.18	5.18	5.18	5.18	5.18	5.18	5.18	5.18	5.18
$\mathbf{k_{bg}}$	0.40	0.37	0.34	0.31	0.27	0.24	0.21	0.18	0.15	0.11	0.08	0.05
$\mathbf{Z_E}$	9.3	9.99	10.7	11.6	12.7	13.9	15.7	17.9	20.9	24.8	30.7	37.9
$\mathbf{Z_S}$	3.51	3.81	3.93	4.36	4.92	5.40	6.14	7.25	8.78	11.5	15.7	24.0
$\mathbf{Z_N}$	8	9	9	10	11	12	14	15	18	22	27	34

Appendix B, Table 2: Predicted variations in euphotic, nutricline, and Secchi depth as a function of salinity in a gradient from NCW_{24} to NAW_{35} in the present

‰	24	25	26	27	28	29	30	31	32	33	34	35
κ	5.18	5.18	5.18	5.18	5.18	5.18	5.18	5.18	5.18	5.18	5.18	5.18
$\mathbf{K_{bg}}$	0.49	0.45	0.40	0.36	0.32	0.281	0.24	0.199	0.16	0.12	0.08	0.04
$\mathbf{Z_E}$	7.97	8.59	9.26	10.07	11.09	12.40	14.0	16.3	19.6	24.6	32.3	41.4
$\mathbf{Z_S}$	2.90	3.16	3.49	3.89	4.13	4.79	5.45	6.54	8.16	11.08	16.97	29.8
$\mathbf{Z_N}$	7	8	8	9	10	11	12	14	17	21	28	38

Appendix B, Table 3: Predicted variations in euphotic, nutricline, and Secchi depth as a function of salinity in a gradient from NCW_{24} to NAW_{35} in a future scenario

‰	24	25	26	27	28	29	30	31	32	33	34	35
κ	5.18	5.18	5.18	5.18	5.18	5.18	5.18	5.18	5.18	5.18	5.18	5.18
$\mathbf{K_{bg}}$	0.79	0.72	0.65	0.584	0.516	0.448	0.38	0.312	0.24	0.176	0.108	0.04
$\mathbf{Z_E}$	5.46	5.9	6.32	6.96	7.64	8.54	9.8	11.4	13.9	17.9	25.8	40.3
$\mathbf{Z_S}$	2.06	2.2	2.46	2.73	2.74	3.14	3.7	4.27	5.36	7.35	12.0	27.1
$\mathbf{Z_N}$	5	6	6	6	7	8	9	10	12	16	23	36